environments

Article

Dynamics of Mercury Distribution: Environmental and Hydrogeochemical Assessment of Artisanal and Small-Scale Gold Mining Impacts in the Upper Caquetá River Basin, Colombia

Saray Karina Gualteros-Esguerra [1], Nelson Fernando Niño-Gutiérrez [2], Fernando Casanoves [3,4], Mónica Sirley Celis-Granada [5], César Jaramillo-Páez [2] and Lis Manrique-Losada [1,*]

[1] Grupo de Investigación Materiales, Ambiente y Desarrollo (MADE), Facultad de Ciencias Básicas, Universidad de la Amazonia, Carrera 31 No. 17-45, Florencia 180001, Colombia; s.gualteros@udla.edu.co
[2] Grupo de Investigación Química Aplicada y Procesos Ecológicos (QUAPE-UT), Facultad de Ciencias, Universidad del Tolima, Ibagué 730006, Colombia; nfninog@ut.edu.co (N.F.N.-G.); cajaramillopa@ut.edu.co (C.J.-P.)
[3] CATIE—Tropical Agricultura Research and Higher Education Center, Turrialba 30501, Costa Rica; casanoves@catie.ac.cr
[4] Doctorado en Ciencias Naturales y Desarrollo Sustentable, Facultad de Ciencias Agropecuarias, Universidad de la Amazonia; Florencia 180001, Colombia
[5] Grupo de Investigación en Fauna Silvestre, Facultad de Ciencias Básicas, Universidad de la Amazonia, Carrera 31 No. 17-45, Florencia 180002, Colombia; m.celis@udla.edu.co
* Correspondence: l.manrique@udla.edu.co

Abstract

Artisanal and small-scale gold mining contributes to mercury contamination in tropical rivers, but its distribution across environmental compartments remains insufficiently characterized in the upper Caquetá River basin, Colombia. Total mercury (THg) was quantified in 50 water samples, 50 sediment samples from eight sites, and 123 fish representing 48 species or morphospecies and four trophic guilds. Sampling covered high-water (May) and low-water (November) phases in 2024. Physicochemical, geochemical, mineralogical, and microstructural were analyzed with linear models, Spearman correlation, and principal components analysis to assess mercury distribution and associated environmental factors. Water THg reached 7.14 µg/L, with 60% of samples exceeding the US EPA chronic aquatic-life criterion. Sediment THg ranged from 1.55 to 176.00 µg/kg dry weight and increased significantly during low water at mining-affected sites, showing associations with fine particles, organic matter, and Fe-, Al-, and Mn-bearing phases. Fish THg ranged from 58.8 to 4324.5 µg/kg dry weight, with significant differences associated with hydrological phase and trophic guild; carnivores and piscivores exhibited higher concentrations. Mercury distribution was compartment-specific and hydrologically modulated, supporting targeted monitoring of sediments and high-trophic-level fish in mining-affected Amazonian river systems.

Keywords: total mercury; artisanal gold mining; hydrogeochemical characteristics; trophic bioaccumulation in fish; sediment-Hg interaction; Colombian Amazon river

Academic Editors: Patrícia Gomes, Charles A. Cravotta, Mehrez Hermassi

Received: 11 October 2026
Revised: 18 November 2026
Accepted: 20 November 2026
Published: 24 November 2026

Copyright: © 2026 by the authors. Licensee MDPI, Basel, Switzerland. This article is an open access article distributed under the terms and conditions of the Creative Commons Attribution (CC BY) license.

1. Introduction

Mercury (Hg) is a persistent global contaminant that can be transported among the atmosphere, water, sediments, and biota, and is recognized by the World Health Organization as a chemical of major public-health concern [1]. The Minamata Convention established a legally binding international framework to reduce Hg emissions and releases, including those associated with artisanal and small-scale gold mining (ASGM), which remains one of the world's largest anthropogenic sources of Hg [2]. In aquatic organisms, Hg exposure can disrupt neurological, oxidative, endocrine, and reproductive processes; in humans, chronic exposure—particularly to methylmercury through fish consumption—is associated with neurodevelopmental, cardiovascular, immune, and neuromotor effects. Fetuses, children, and women of reproductive age are among the most vulnerable groups [3–5].

In tropical fluvial ecosystems such as the Amazon basin and the Caquetá River, hydrological pulses regulate mercury (Hg) transport, sedimentation, remobilization, and biological exposure [6,7]. River sediments constitute dynamic geochemical compartments that integrate inputs from the catchment and act simultaneously as sinks, reservoirs, and potential secondary sources of Hg. Their capacity to retain or release this contaminant depends on several factors, including hydraulic energy, particle-size distribution, organic matter content, and mineralogical composition. Fine-grained fractions, clay minerals, aluminosilicates, and iron, aluminum, and manganese oxides and hydroxides provide reactive surfaces that favor Hg adsorption and retention [4,8,9]. High-water phases increase discharge, promoting particle resuspension and downstream transport, while low-water conditions enhance the deposition of fine fractions and organic matter [6,7]. Consequently, variations in sediment composition and physicochemical conditions can influence Hg partitioning between the aqueous and solid phases, affecting its environmental mobility and potential bioavailability.

Amazonian rivers also support highly diverse fish communities characterized by complex trophic structures and ecological interactions. Fish play an essential role in aquatic food webs and are particularly relevant for assessing Hg contamination because they integrate environmental exposure over time through water, suspended particles, sediments, and dietary pathways. Mercury accumulation in fish is influenced by species-specific ecological characteristics, feeding habits, trophic position, habitat use, and hydrological conditions. Predatory and piscivorous species may exhibit higher Hg concentrations due to bioaccumulation and biomagnification along food webs [5,10]. In the Amazon region, seasonal flood pulses modify habitat connectivity, food availability, fish movements, and trophic interactions, thereby influencing Hg exposure and accumulation in aquatic organisms [6,11,12]. These processes are particularly relevant in rivers such as the Caquetá, where fish constitute an important source of protein and a fundamental component of the livelihoods and cultural practices of riverine and Indigenous communities.

The upper Caquetá River basin, located in the Colombian Amazon, is subject to intensive river dredging and mercury-assisted alluvial gold extraction [13]. While mercury exposure through fish consumption has been documented in parts of the Colombian Amazon [5,9,10,13,14], comprehensive baseline data on total mercury (THg) concentrations in abiotic (water and sediments) and biotic (fish) matrices of the upper Caquetá River remain limited. Furthermore, relatively few studies have simultaneously investigated the relationships between Hg concentrations and the physicochemical characteristics of water, as well as the physical, geochemical, and mineralogical properties of sediments, under contrasting hydrological conditions. Understanding these relationships is essential because the physical and chemical characteristics of water and sediments can influence Hg mobility, retention, transport, and potential transfer to

https://doi.org/10.3390/environments13120643

aquatic organisms. Likewise, evaluating correlations among environmental compartments can provide insights into the processes governing Hg distribution and interactions within riverine ecosystems. Addressing these knowledge gaps is particularly important for Amazonian communities whose livelihoods, cultural practices, and dietary protein intake rely heavily on local fisheries [9,13].

The objective of this study was to conduct an integrated environmental and hydrogeochemical assessment of total mercury distribution in water, sediments, and fish in the upper Caquetá River basin during contrasting high-water and low-water hydrological phases. This assessment combined physicochemical, geochemical, mineralogical, microstructural, and ecological analyses to identify the environmental factors associated with Hg distribution and retention, and to evaluate correlations among mercury concentrations, abiotic environmental characteristics, and biological compartments, thereby providing a comprehensive understanding of mercury dynamics in an artisanal and small-scale gold mining-impacted Amazonian river system.

2. Materials and Methods

2.1. Study Area

The study was conducted in the upper Caquetá River basin, in the departments of Caquetá and Putumayo, Colombia, along the river corridor extending from Villa Garzón to Mecaya and Las Delicias, including the confluence of the Mandur and Caquetá rivers near Puerto Guzmán (Figure 1). The Caquetá River is approximately 2820 km long, and the evaluated upper-basin sector is part of the Apical, Direct Tributaries, and Orteguaza subsystems. Mining intensity and site selection were supported by cartographic information and data generated by the project 'Analysis of the socio-environmental impact of mercury and sustainable technologies for its removal in the upper Caquetá-Putumayo River basin' (BPIN 2022000100050).

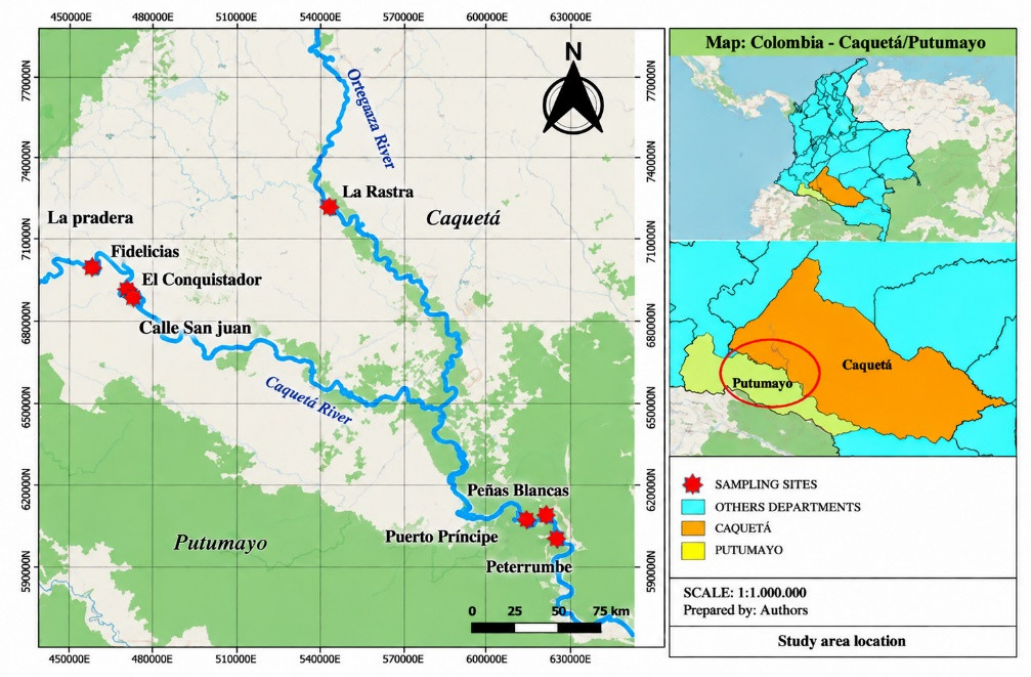


Figure 1. Spatial distribution of the eight sampling sites in the upper Caquetá River basin, Colombia. The map on the (**left**) shows the distribution of the sampling sites while the panels on the (**right**) display study area location within Caquetá-Putumayo Departments—Colombia. Source: Prepared by the authors.

Eight sites were evaluated: seven associated with active ASGM (El Conquistador, Peñas Blancas, Peterrumbe, Calle San Juan, La Pradera, Puerto Príncipe, and Fidelicia) and one reference site without recent local mining activity (La Rastra, a tributary of the Orteguaza River). Water and sediment samples were collected at all eight sites to maximize spatial coverage. Fish sampling was restricted to El Conquistador, Peñas Blancas, Peterrumbe, and La Rastra because the sampling design prioritized concurrent measurements of all three matrices in three impacted settings and one reference setting; the remaining sites expanded the spatial assessment of the abiotic matrices. This design should be interpreted as an integrated reference-impact comparison rather than as equivalent biological coverage across all eight locations.

Sampling was conducted under two hydrological conditions: the high-water phase (E1, May 2024) and the low-water phase (E2, November 2024). The E1 and E2 labels represent hydrological phases (E1: high water; E2: low water). Complementary E1 sampling at El Conquistador, Peñas Blancas, and Peterrumbe provided concurrent water, sediment, and fish data comparable with E2. The final analytical dataset comprised 50 water samples, 50 sediment samples, and 123 fish.

2.2. Sample Collection and Preparation

The sampling strategy was designed to preserve matrix-specific characteristics while maintaining spatial correspondence among water, sediment, and fish at the four integrated sites. The main procedures are summarized below.

2.2.1. Water

Water was collected in 2-L high-density polyethylene containers previously acid-washed. For total mercury determination, a 500-mL aliquot was preserved with 2.5 mL of concentrated HNO_3 and refrigerated at ≤6 °C in a filled and sealed container. The water samples were stored after sedimentation. Two or three samples, distributed spatially, were collected in duplicate for each site and hydrological phase. Complementary E1 samples were included in the final dataset of $n = 50$ [15].

2.2.2. Sediments

Surface sediment samples were collected using either an Ekman dredge or a clean plastic shovel, depending on site access, water depth, and sampling point stability. Sampling locations were selected in the field based on visual and operational criteria, prioritizing depositional areas characterized by accumulations of soft, moist, muddy material typically found in low current-energy environments.

This approach targeted surface sediments with a higher potential for mercury accumulation and retention. Mercury in sediments preferentially associates with fine fractions, such as silts and clays, because of their larger surface area and interactions with clay minerals, aluminosilicates, oxyhydroxides, and fine organic matter [4].

During sampling, visible coarse materials such as gravel, pebbles, coarse sand, and large plant fragments were systematically avoided, as these do not represent the accumulated bottom sediment. Efforts were also made to minimize the loss of fine material during sample handling.

Sediment textural classification was determined through laboratory analyses rather than solely by visual field observation. Field criteria helped select representative surface sediment samples, while comprehensive physical, mineralogical, and geochemical characterizations were conducted in the laboratory.

Approximately 1000 g of each sample was collected in self-sealing plastic bags, which were properly labeled and coded. Samples were refrigerated at 4 °C, without freezing,

during transport to the laboratory, following the preservation and handling guidelines outlined in the IDEAM manual [15].

In the laboratory, each sample was spread on a clean tray to prevent loss of fine material. Samples were oven-dried at 30 °C, sieved, and ground in a porcelain or agate mortar until a fine powder was obtained. This material was subsequently used for mineralogical characterization by X-ray diffraction (XRD) and for major oxide determination by X-ray fluorescence (XRF).

For morphological and compositional analysis using scanning electron microscopy coupled with energy-dispersive X-ray spectroscopy (SEM-EDS), an unground subsample was reserved to preserve the original particle morphology [8].

2.2.3. Fish

Fish were collected at La Rastra, El Conquistador, Peñas Blancas, and Peterrumbe using hand nets and hook-and-line fishing with the support of local fishers and following GTC 25:2023 [16]. A total of 123 individuals representing 48 species or morphospecies and four trophic guilds (detritivores, omnivores, carnivores, and piscivores) were obtained. Specimens were transported at approximately 6 °C, stored at −20 °C, subsequently deep-frozen at −80 °C, freeze-dried, and homogenized to a fine powder. Collection was conducted under ANLA Framework Permit No. 01140 of September 30, 2016, and Universidad de la Amazonia authorization 600.6.668 (April 2024).

2.3. Environmental Characterization

2.3.1. Water-Quality Characterization

Fifteen water-quality variables were determined according to Standard Methods and IDEAM procedures [17]: (1) pH, (2) electrical conductivity, (3) turbidity, (4) total suspended solids, (5) total solids, (6) five-day biochemical oxygen demand, (7) chemical oxygen demand, (8) alkalinity, (9) total hardness, (10) chloride, (11) sulfate, (12) ammonium, (13) nitrate, (14) orthophosphate, and (15) total phosphorus. Analytical method codes and units are provided in Table A1 [17].

2.3.2. Geochemical, Mineral-Phase, and Microstructural Characterization of Sediments

Sediment characterization included pH and electrical conductivity, organic carbon and organic matter determined by Walkley-Black wet oxidation (NTC 5403:2021), and particle-size distribution determined by the Bouyoucos hydrometer method (NTC 6299:2018).

Mineral phases and their relative abundances were determined by X-ray diffraction using a MiniFlex diffractometer operated at 40 kV and 30 mA, equipped with a D/teX Ultra detector and a Ni filter to suppress Cu Kβ radiation. Cu $K\alpha_1$ radiation (λ = 1.5405 Å) was used, with a scan speed of 10° min^{-1}, a step size of 0.01°, and a 2θ range of 2–90°. reference patterns from the ICDD PDF-4/Minerals 2025 database. Its relative abundances were estimated semi-quantitatively using the Reference Intensity Ratio (RIR) method, based on the RIR values provided in the corresponding crystallographic reference cards. Major-oxide composition (SiO_2, Al_2O_3, Fe_2O_3, CaO, MgO, TiO_2, MnO, P_2O_5, BaO, and K_2O) was determined by X-ray fluorescence using a NEX QC+ QuantEZ instrument, with 30-s detection times and voltages of 6.5, 30, and 50 kV for low-, medium-, and high-atomic-number elements, respectively.

Particle morphology and localized elemental composition were analyzed by field-emission scanning electron microscopy coupled with energy-dispersive X-ray spectroscopy (FESEM-EDS), using a Thermo Fisher Scientific Scios 2 LoVac dual-beam instrument and an UltraDry EDS detector (129 eV, 30 mm^2) (Brno, Czech Republic). The microscope provided resolutions of 0.7 nm at 30 kV in STEM mode and 1.4 nm at 1 kV in

FESEM mode. XRD, XRF, and FESEM-EDS analyses were applied to representative samples from the lower and upper percentiles of sediment THg and to samples from the reference site.

2.4. Total Mercury Determination and Quality Assurance

Total mercury (THg) was quantified in water, sediment, and freeze-dried fish muscle samples using an RA-915 LAB direct mercury analyzer (Lumex Instruments), based on direct thermal decomposition and atomic absorption spectrometry with Zeeman background correction. The procedure is compatible with US EPA Methods 7473, 30B, and PS12B. All determinations were performed duplicate.

For the analysis:

- Water: Water samples did not require pretreatment. The aliquot was placed directly into a porcelain crucible for combustion and subsequent measurement. 1000 µL (1 mL) aliquots of water were processed, without filtration, using the operating mode for water.
- Sediments: 0.200 g of dried, homogenized, pulverized sediment and were analyzed using the Soil operating mode.
- Fish: 0.100 g of freeze-dried muscle tissue were analyzed using the Soil operating mode. Because THg concentrations in fish were determined in freeze-dried tissue and are expressed on a dry-weight (d.w.) basis, whereas Resolution 122 of 2012 establishes its regulatory limits on a wet-weight (w.w.) basis, unit conversion was required to enable direct comparison. Assuming a reference muscle moisture content of 78%, the wet-weight concentration was calculated as follows:

$$C_{ww} = {C_{dw}}/{4.545}$$

Instrument calibration was performed over the 0–20 ng Hg range, yielding coefficients of determination of $r^2 \geq 0.999$. As part of analytical quality assurance, one blank was analyzed every 10 samples (all blanks showed mercury levels below LOQ/2. Under these conditions, the readings were then taken). Accuracy was verified using matrix-specific certified reference materials (CRM): a certified High-Purity Standards Hg solution in 2% HNO_3 for water, IAEA-475 for sediment, and IAEA-436 (tuna fish flesh homogenate) for fish muscle.

Method validation included repeatability, accuracy, limits of detection (LOD) and quantification (LOQ), recovery, and expanded uncertainty (Table 1). LOD and LOQ values were, respectively, 0.27 and 0.82 ng for water; 0.20 and 0.62 ng for sediment; and 0.027 and 0.083 ng for fish tissue. Recoveries ranged from 94% to 107%, with coefficients of variation below 5% (Table 1). Duplicate determinations were considered acceptable when the coefficient of variation (CV) was ≤5%; otherwise, the analysis was repeated. For statistical treatment, results below the LOQ were replaced with LOQ/2.

Table 1. Matrix-specific validation parameters for total mercury determination.

Matrix	LOD (ng)	LOQ (ng)	Expanded Uncertainty (ng)	Certified Reference Material	Certified Hg Value	CRM Uncertainty
Water	0.27 ± 0.05	0.82 ± 0.16	±0.16	High-Purity Standards Hg solution	1000 mg/L	±5 mg/L
Sediment	0.20 ± 0.04	0.62 ± 0.14	±0.06	IAEA-475	0.0299 mg/kg	±0.0023 mg/kg
Fish	0.027 ± 0.005	0.083 ± 0.015	±0.053	IAEA-436	4.26 mg/kg	±0.36 mg/kg

2.5. Statistical Analysis

Descriptive statistics were calculated by site and hydrological phase. We use an analysis of variance with lineal models (LM) to evaluate the effect of sampling site, hydrological phase, and their interaction on total mercury and environmental variables. Normality and homogeneity of variance were assessed using the Shapiro–Wilk test and residuals vs. predicted graph, respectively. When the variances were heterogeneous, we modelled the variance-covariance matrix using variance identifier (VarIden) function. The best model selection was based in AIC and BIC criteria. We used Fisher LSD ($p < 0.05$) to compare treatment means.

Associations were evaluated using Spearman rank correlations. Principal component analyses (PCA) were performed on standardized variables separately for water and sediments in E1 and E2, and jointly for the four sites with complete information for all three matrices.

THg in fish was compared among trophic guilds using the Kruskal–Wallis test, followed by pairwise Mann–Whitney comparisons with Holm-Bonferroni correction. Shannon–Wiener and Simpson indices were used to describe fish diversity. Jaccard coefficients described compositional similarity, and Ward hierarchical clustering was applied to the site-phase dissimilarity matrix. The final dendrogram had a cophenetic correlation of 0.700. Analyses were performed in InfoStat v.2020 with $\alpha = 0.05$.

3. Results

Results are showed by environmental compartment and subsequently integrated across matrices (Table 2). Statistical effects are distinguished from descriptive trends, and mechanistic interpretations are presented as associations because the study quantified total mercury rather than individual Hg species.

Table 2. Summary of total mercury concentrations and main statistical results.

Matrix	n	Range	High-Water Mean	Low-Water Mean	Main Model Result	Regulatory Comparison *
Water (µg/L)	50	0.41–7.14	0.98 ± 1.46	1.54 ± 0.61	Site, phase, and interaction: not significant ($p > 0.05$)	12% > 2 µg/L; 50% > 1 µg/L; 60% > 0.77 µg/L
Sediment (µg/kg dw)	50	1.55–176.00	32.31± 18.53	91.15± 48.81	Phase F = 72.04; site F = 6.43; interaction F = 6.46; all $p \leq 0.0001$	98% below TEL = 170 µg/kg; all below PEL = 486 µg/kg
Fish (µg/kg dw)	123	58.80–4324.50	—	—	Phase F = 5.81; $p = 0.0175$; site F = 2.51; $p = 0.0619$	12 fish >0.5 mg/kg ww; maximum in predators = 0.951 mg/kg ww

* TEL: Threshold Effect Level, according to the Interim Sediment Quality Guidelines and PEL: Probable Effect Level, according to the Interim Sediment Quality Guidelines (ISQG) ([18]).

3.1. Water Quality in the Caquetá River

The results of the physicochemical characterization of the water are presented in Table A2. The pH at the sampling sites ranged from slightly acidic to slightly basicity (5.16–7.88), with higher values during the high-water phase (7.48 ± 0.29) than during the low-water phase (6.48 ± 0.07). La Rastra showed the lowest electrical conductivity (19.50 ± 2.25 µS/cm) and alkalinity (11.00 ± 2.94 mg/L $CaCO_3$), reflecting a lower ionic load and lower anthropogenic contribution compared with the impacted sites [14].

Total suspended solids showed high overall variability, with maximum values at El Conquistador during both hydrological phases (39.43 ± 18 mg/L), associated with the erosion of natural material and the mechanical removal of bed material due to anthropogenic intervention, such as dredging operations. Likewise, La Rastra recorded

high turbidity (73.38 ± 12.38 NTU) higher than the turbidity at any point along the Caquetá River (Fidelicias E1 39.36 ± 5.97), indicating that the natural dynamics of the Orteguaza River drive the transport of high levels of particulate matter, in contrast to the material contributed by mining activity on the Caquetá River [19].

Total solids at El Conquistador reached concentrations of 254.31 ± 48.13 mg/L, well above the overall mean (113.44 ± 66.09 mg/L). Likewise, the concentration of total suspended solids at most sampling sites represented up to 20% of the total solids content, allowing total dissolved solids (proportional to conductivity) to be identified as the main contributors to total solids in the river water. Electrical conductivity was generally moderate due to the load of mineral salts and nutrients eroded from the river's headwaters (the Andes) and enriched by its tributaries across the Amazonian lowlands. The highest values were recorded at Fidelicias (117.04 ± 30.63 μS/cm) and La Pradera (59.60 ± 10.51 μS/cm), while alkalinity and total hardness also reached their highest levels at Fidelicias in E2 (69.81 ± 14.34 and 60.74 ± 10.83 mg/L $CaCO_3$, respectively), reflecting differential buffering capacity among sites that may modulate the chemical stability of metals in solution [20].

Marked differences between hydrological phases were observed in NH_4^+ concentrations, showing levels of 3.37 ± 0.68 during the E1 versus levels of 0.88 ± 0.20 mg/L during the E2 phase. Cl^- concentrations show the same trend (105.25 ± 21.83 mg/L in E1 versus 28.65 ± 5.87 mg/L in E2). Overall, nutrient and other ion levels were moderately high and were attributed to intense erosion of mountain soil and material transport. The latter is enhanced during the high-water hydrological phase. BOD_5 showed higher values during the low-water phase (6.48 ± 1.38), indicating mesosaprobic environments with a predominance of oxidative processes.

Total mercury concentrations in water (THg-A) ranged from 0.28 to 7.14 μg/L, with an overall mean of 1.42 ± 0.36 μg/L; El Conquistador recorded the highest values (5.56 ± 1.19 μg/L), followed by Peñas Blancas (2.23 ± 0.45 μg/L) and Puerto Príncipe (1.88 ± 0.38 μg/L). In contrast, La Rastra, a reference site without alluvial gold-mining activity, presented the lowest mean THg concentration (0.84 ± 0.26 μg/L).

These spatial variations are particularly relevant when assessed against the regulatory thresholds established to protect human health and aquatic life. Compared with the technical criterion established in Decree 3930 of 2010 (2 μg/L) [21], 12% of the samples exceeded this threshold (6/50). Exceedances were identified at El Conquistador during the E1 period and at Peñas Blancas, La Pradera, and Puerto Príncipe during the E2 period. Because riverine communities in the upper Caquetá River basin routinely consume untreated river water, Resolution 2115 of 2007 (1 μg/L) [22] was also included as a comparison threshold. Against this value, 50% of the samples (25/50) exceeded the threshold, highlighting the magnitude of the potential health risk to which these populations are exposed.

A single measurement of 7.14 μg/L at El Conquistador during the high-water period also exceeded the WHO guideline value for drinking water (6 μg/L) [23], coinciding with active dredging operations in the area at the time of sampling. La Rastra also exceeded the threshold established by Resolution 2115 of 2007 during the low-water period (mean: 1.37 ± 0.96 μg/L), indicating contaminant transport at the basin scale [24]. Relative to the US EPA chronic criterion for the protection of aquatic life (0.77 μg/L) [25], 60% of all samples exceeded the threshold (30/50), indicating a sustained ecotoxicological risk to aquatic biota in the upper Caquetá River basin.

3.2. Physicochemical Control of Mercury in Caquetá River Water

The correlation between total mercury and water-quality parameters in the Caquetá River is presented in Figure 2. Total mercury in water (THg-A) showed a significant

positive correlation with BOD_5 ($p < 0.001$), indicating that higher THg-A concentrations were associated with a greater biodegradable organic-matter load. This result suggests that organic matter in the water may promote mercury persistence and transport through the formation of organic and colloidal complexes, which modify its partitioning among dissolved, particulate, and sedimentary fractions. Dissolved organic matter, particularly that containing thiol functional groups, has been shown to control mercury speciation and bioavailability in aquatic systems, potentially facilitating its subsequent incorporation into food webs under suitable environmental conditions [26,27]. Therefore, the correlation between THg-A and BOD_5 should be interpreted as an indicator of coupling between mercury and biodegradable organic-matter load rather than as isolated evidence of direct causality.

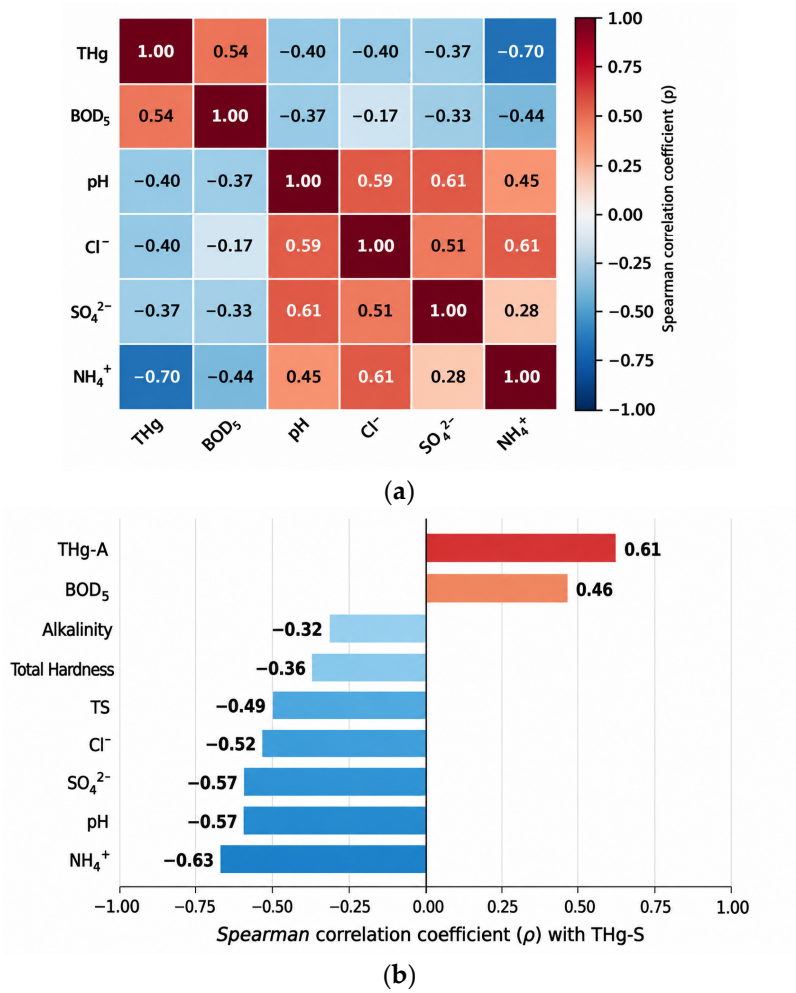


Figure 2. (**a**) Spearman correlation matrix between total mercury in water (THg-A) and water-quality parameters in the upper Caquetá River basin; and (**b**) Spearman correlation between total mercury in sediments (THg-S) and water-quality parameters including THg-A, in the upper Caquetá River basin.

In contrast, THg-A showed significant negative correlations with pH ($p < 0.001$), chlorides ($p < 0.001$), sulfates ($p = 0.01$), and ammonium ($p < 0.001$). Higher THg-A concentrations were associated with lower pH and lower concentrations of these ions. From a geochemical perspective, pH, chlorides, sulfates, and other inorganic ligands can modify mercury speciation, its complexation with organic and inorganic ligands, its affinity for suspended particles, and its redistribution between the aqueous phase and the sediment matrix. Consequently, this correlation suggests the presence of a hydrochemical

gradient that conditions the mobility and partitioning of THg within the aquatic system [9,28].

To identify the main physicochemical gradients associated with the distribution of total mercury in water (THg-A), a principal component analysis (PCA) was performed for each hydrological phase (E1 and E2) (Figure 3). Interpretation was based on vector orientation, the proximity among variables, and the relative position of sampling sites in the plane defined by the first two principal components.

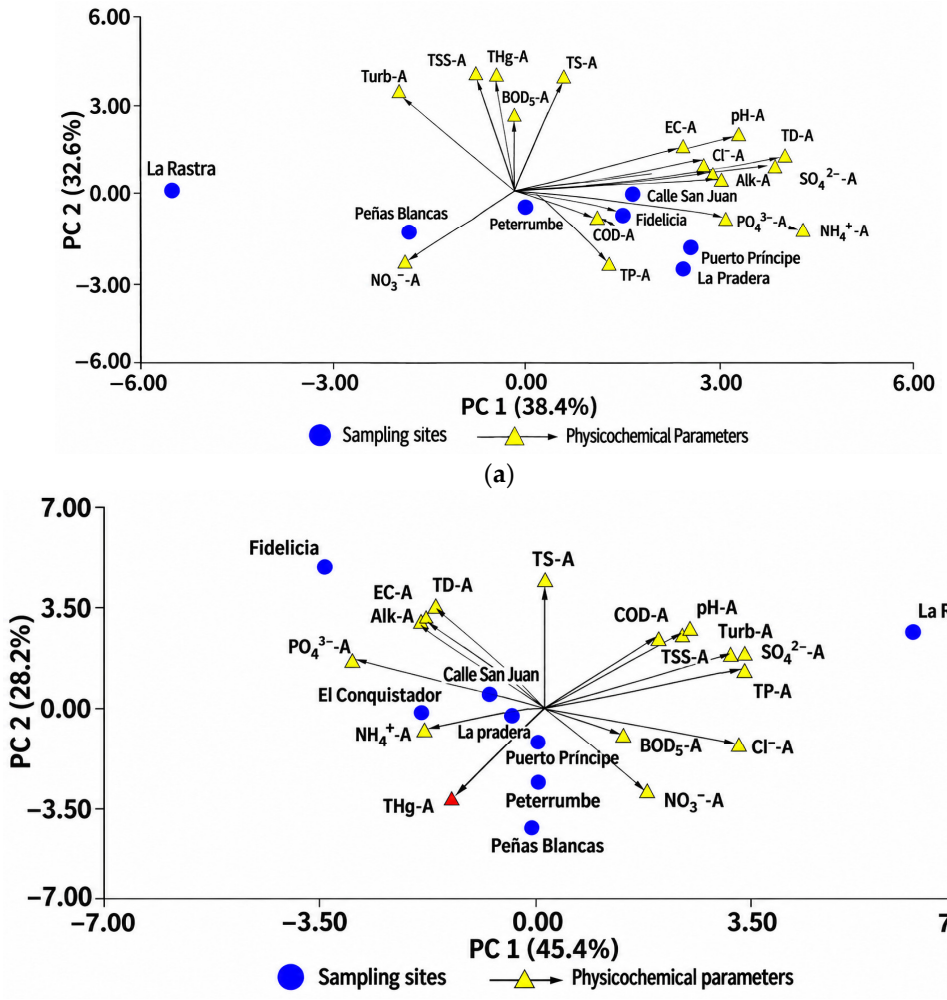


Figure 3. Principal component analysis (PCA) of total mercury concentrations in water (THg-A) and water quality parameters during: (**a**) the high-water hydrological phase (E1) and (**b**) the low-water hydrological phase (E2), at sampling sites in the upper Caquetá River basin.

During the high-water hydrological phase (E1), the first two principal components explained 71.0% of the total system variability, with 39.6% accounted for by PC1 and 32.6% by PC2.

In E1 (Figure 3a), the THg-A vector was located in the upper sector of the biplot, close to TSS-A, TS-A, Turb-A, and BOD_5-A. This arrangement indicates that, during high-water, the variability of total mercury in the water column was primarily associated with TSS, TS, turbidity, and biodegradable organic matter loads. This behavior is consistent with the high-water hydrological phase, characterized by greater hydraulic energy, during which increased discharge may promote resuspension of bed material (suspended material, colloids, and organic complexes), bank erosion, and transport of fine particles into the

water column. Therefore, THg-A was primarily related to a gradient of suspended particulate and organic transport, facilitating its mobilization.

El Conquistador was located as an extreme point toward positive PC2, in the same direction as the group formed by THg-A, TSS-A, TS-A, Turb-A, and BOD_5-A. This position indicates that El Conquistador exhibited a differentiated condition during high water, characterized by a greater relative influence of total mercury in water and suspended material. This result is consistent with the observation of dredging activity during sampling and suggests that dredging, by removing bed material and increasing turbidity, could promote the incorporation of THg-bearing particles into the water column.

In contrast, parameters associated with dissolved species in the water (ionic composition), such as pH-A, EC-A, alkalinity, total hardness, SO_4^{2-}-A, Cl^--A, and NH_4^+-A, were mainly grouped toward the positive end of PC1, separated from the THg-A vector. This arrangement indicates that, during E1, THg-A was more closely related to solid particles and turbidity variables than to the dissolved ionic composition of the water.

Peñas Blancas was located toward the negative PC2 sector, close to the NO_3^--A vector, evidencing a hydrochemical condition distinct from that observed at El Conquistador. This separation suggests that Peñas Blancas was less associated with the THg-A—solid particles—turbidity gradient during high water and more closely related to a specific nitrate signal. Overall, the E1 PCA shows that the main THg-A pattern was associated with a physical particle-transport gradient, with El Conquistador representing the site most characteristic of this condition.

During the low-water hydrological phase (E2), the first two principal components explained 73.6% of the total variability, with 45.4% for PC1 and 28.2% for PC2, as shown in Figure 3b. This result indicates that the PCA adequately represented the main physicochemical gradients of the water during the lower-discharge period.

In E2, the multivariate pattern changed relative to E1. The THg-A vector shifted toward the lower-left quadrant of the biplot and became separated from the variables related to suspended solids, turbidity, and total solids, which were located toward the positive side of PC1. This separation indicates that, during low water, THg-A variability was not dominated by the same particulate gradient observed during high water. Therefore, the PCA reveals a seasonal change in the relationship between total mercury in water and the physicochemical parameters of the system.

The position of THg-A in E2 was close to the sector where NH_4^+-A was located. Ammonium may be associated with organic-matter mineralization processes, lower oxygenation, or greater local interaction between the water column and deposited bottom material. Therefore, the proximity between THg-A and NH_4^+-A suggests that, during low water, total mercury may have been more strongly influenced by local hydrochemical processes than by direct transport of suspended solids.

From a biogeochemical perspective, this association may be interpreted as an indirect signal of environmental conditions that promote changes in THg mobility, complexation, and availability in the water column. Dissolved organic matter, reduced functional groups, sulfates, chlorides, and oxygenation conditions can modify mercury behavior in aquatic systems [26,28,29].

Peterrumbe and Peñas Blancas were located close to the THg-A sector during E2. This arrangement suggests that both sites exhibited conditions more closely related to the mercury pattern observed during low water. This result is relevant because Peterrumbe and Peñas Blancas correspond to areas influenced by alluvial gold mining and hydrological dynamics that may favor lower turbulence, longer water residence time, or greater local interaction between the water column and deposited material. Consequently, the PCA suggests that, during E2, THg-A at these sites may have responded to local processes different from the particulate transport that dominated in E1.

La Rastra, a reference site without direct mining activity, was located at the positive end of PC1 and associated with Turb-A, TSS-A, pH-A, SO_4^{2-}-A, and TP-A. This position indicates that La Rastra exhibited a differentiated physicochemical condition during low water, characterized by a stronger relationship with suspended solids, turbidity, and some dissolved constituents. However, because it was not associated with the THg-A vector, this condition should not be interpreted as a signal of mercury contamination, but rather as an expression of the natural variability of the reference system, possibly related to the natural dynamics of the Orteguaza River, its natural fine-solid load, or baseline hydrochemical differences.

Based on the findings, a pattern of seasonal THg accumulation can be identified at mining-impacted sites, suggesting the creation of conditions that lead to significantly higher THg levels in the aquatic biota of these locations. The magnitude and spatiotemporal distribution of these concentrations in the water column raise the question of the extent to which mercury accumulates and redistributes within the sediment matrix, which acts simultaneously as a sink, a reservoir, and a potential source of the metal for aquatic biota.

3.3. Total Mercury in Sediments and Geochemical Controls

THg in sediments ranged from 1.55 to 176.00 μg/kg dry weight (overall mean: 59.37 ± 46.15 μg/kg) and was substantially higher in E2 (91.15 ± 48.81 μg/kg) than in E1 (32.31 ± 18.53 μg/kg). Evaluating sediments against international standards, total mercury concentrations ranged from 1.55 to 176.00 μg/kg (mean: 59.37 ± 46.15 μg/kg; n = 50), using the Interim Sediment Quality Guideline (ISQG) [18], as Colombian regulations are lacking. The Threshold Effect Level (TEL = 170 μg/kg) and Probable Effect Level (PEL = 486 μg/kg) were applied. Although 98% of samples were below the TEL, Peterrumbe during low water averaged 169.0 ± 6.6 μg/kg, nearing this threshold, and Peñas Blancas had 118.3 ± 27.5 μg/kg. Both sites are in a transition zone where adverse effects on benthic biota are possible. Mercury increased seasonally only where mining occurs, with concentrations rising three- to five-fold between high and low water, confirming extractive activity as the main driver of mercury accumulation.

Forty-nine of the 50 sediment samples were below the CCME threshold effect level (TEL, 170 μg/kg dry weight), and all were below the probable effect level (PEL, 486 μg/kg). Peterrumbe approached the TEL during E2 (169.0 ± 6.6 μg/kg), whereas Peñas Blancas reached 118.3 ± 27.5 μg/kg. Values below the TEL do not demonstrate absence of risk, although adverse effects on benthic organisms are expected to occur infrequently. Seasonal increases and proximity to the TEL identify Peterrumbe and Peñas Blancas as monitoring priorities.

Sediment THg was positively correlated with Al_2O_3 (r = 0.40; p = 0.0039), Fe_2O_3 (r = 0.37; p = 0.0076), MnO (r = 0.42; p = 0.0027), and THg in water (r = 0.62; $p < 0.0001$). In contrast, SiO_2 was negatively correlated with sediment THg (r = −0.40; p = 0.0041). These patterns are consistent with the greater sorption sites of metal oxides, clay surfaces, and organic matter relative to quartz-dominated materials [8,14]. The correlation between THg in water and sediments (r = 0.62 y $p < 0.0001$ in the integrated site-phase dataset) further indicates active exchange between the water column and sediment compartment.

Sediment PCA revealed phase-dependent associations. During E1, THg covaried with clay, Al_2O_3, Fe_2O_3, Fe, and MnO, consistent with retention on sorption sites oxide surface and fine particles (Figure 4a). During E2, THg shifted toward organic matter, organic carbon, and clay, suggesting that deposition under low-discharge conditions increased the relative importance of organomineral retention (Figure 4b). These are empirical associations and should not be interpreted as evidence that one exclusive

sorption mechanism replaced another; multiple binding processes likely operated simultaneously.

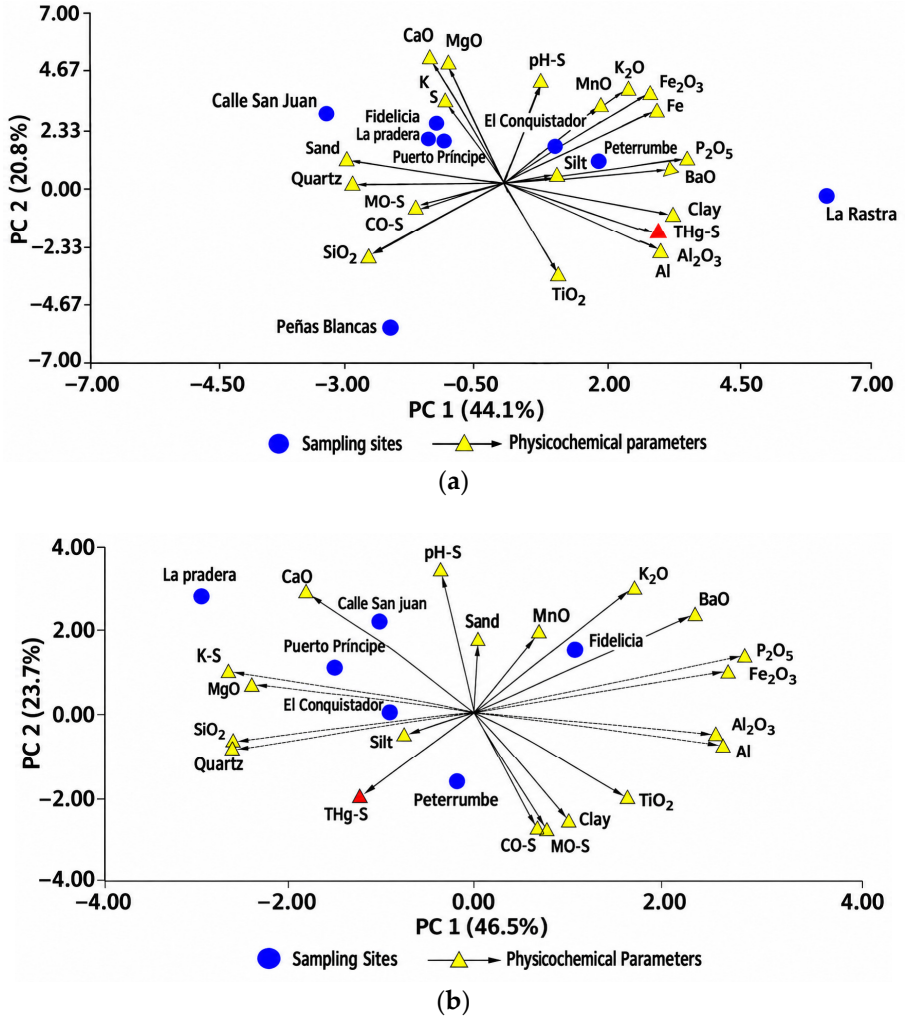


Figure 4. PCA biplot of total mercury in sediments and geochemical and mineral-phase characteristics during: (**a**) E1 and (**b**) E2.

Microstructural observations supported the multivariate patterns. The CSJR2 sample from the lower E1 percentile (7.60 µg/kg) was dominated by quartz (69.8%), had low organic matter content (1.38%), and consisted of coarse, angular particles with limited aggregation. The PTR3 sample from the upper E2 percentile (162.90 µg/kg) had higher clay content, Al_2O_3 (18.1%), Fe_2O_3 (9.15%), and organic matter (3.19%), and showed cohesive fine-grained aggregates. The P10-to-P90 contrast was 4.0-fold in E1 and 6.2-fold in E2, consistent with greater accumulation in fine, reactive material during low-water conditions.

This mixture creates optimal conditions for THg-S retention, as organomineral aggregates and sorption sites concentrate mercury in low-energy sediments. Overall, results confirm that THg-S accumulation in the upper Caquetá River basin depends on the ratio of reactive to less-reactive mineral phases. Sediments rich in quartz and coarse particles retain less mercury, while those with more organic matter, clays, Al_2O_3, Fe_2O_3, and fine aggregates retain more. Low-water periods promote fine material deposition and increased THg-S retention, especially in areas like Peterrumbe. Mercury accumulation in sediment varies with hydrological phase, texture, organic matter, and mineralogy [8,27,30,31].

The XRD patterns of the representative sediment samples collected during the two hydrological periods are presented in Figure 5. Quartz was identified in all samples, exhibiting its characteristic diffraction reflection at approximately 2θ = 26.7°, assigned to the (101) plane. The additional indexed reflections were consistent with the occurrence of plagioclase, anorthite, clinochlore, and fraipontite, depending on the sampling location and hydrological period. Comparison with the corresponding ICDD reference patterns supported the mineral-phase assignments, while semi-quantitative RIR analysis provided the relative abundances reported in Table 3. Additional XRD patterns are presented in Figure A1.

Table 3. Representative sediment samples selected from the lower and upper percentiles of total mercury. THg-S is expressed in μg/kg dry weight.

Sample/Phase	THg-S	Texture	Mineralogical Composition (Dominant XRD Phases)	Elemental Content as Oxides (Selected XRF Variables)	Organic Content (OM)	SEM Morphology
CSJR2/E1 P10	7.60	Sandy loam	Quartz 69.8%; plagioclase 30.2%	SiO_2 66.9%; Fe_2O_3 8.4%;	OM 1.38%	Coarse, angular particles; low aggregation
PTL1/E1 P90	30.54	Sandy loam	Quartz 52%; plagioclase 48%	Al_2O_3 16.9%; Fe_2O_3 8.6%;	OM 3.40%	Fine particles adhering to surfaces; moderate aggregation
La Rastra/E1	56.22	Sandy clay loam	Plagioclase 23%; clinochlore 19%; quartz 58%	Fe_2O_3 10.1%;	OM 0.95%	Aggregates associated with Fe-rich phases
CSJR2/E2 P10	26.40	Sandy loam	Quartz 70%; anorthite 26.7%; fraipontite 3.32%	Fe_2O_3 8.2%;	OM 1.96%	Fragmented particles; presence of diatoms
PTR3/E2 P90	162.90	Loam	Quartz 62%; plagioclase 38%	Al_2O_3 18.1%; Fe_2O_3 9.15%;	OM 3.19%	Fine cohesive microstructures; high aggregation
La Rastra/E2	24.34	Sandy clay loam	Plagioclase 53%; quartz 21.2%; clinochlore 25.8	Fe_2O_3 13.4%;	OM 3.75%	Fe-rich microaggregates; moderate cohesion

During E1, quartz and plagioclase were identified in both CSJR2 and PTL1, with a higher relative proportion of quartz in CSJR2 (69.8%) than in PTL1 (52%). In contrast, La Rastra exhibited a mineral assemblage comprising quartz (58%), plagioclase (23%), and clinochlore (19%). During E2, the CSJR2 pattern was characterized by quartz (70%), anorthite (26.7%), and a minor contribution from fraipontite (3.32%), indicating a different assemblage of identified phases from that observed during E1. Quartz and plagioclase remained the principal phases in PTR3, whereas La Rastra exhibited a marked change in relative mineral abundance, with plagioclase increasing from 23% to 53%, clinochlore from 19% to 25.8%, and quartz decreasing from 58% to 21.2%. These variations reveal differences in the crystalline mineral assemblages among sediment samples and between hydrological periods, complementing the geochemical and microstructural characteristics summarized in Table 3.

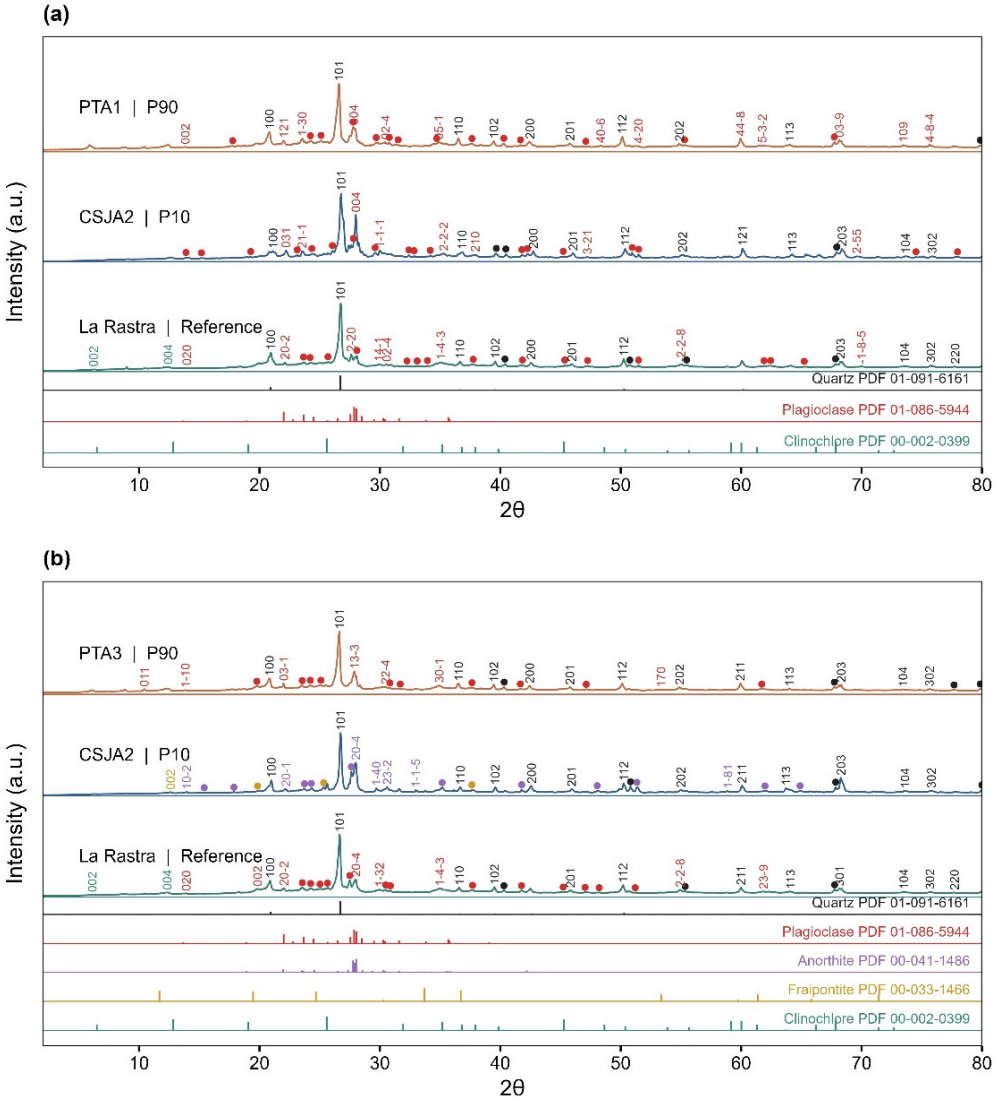


Figure 5. X-ray diffraction patterns of representative sediments during: (**a**) E1 and (**b**) E2.

Integrated XRD and SEM analyses (Figures 5 and 6) revealed distinct sediment characteristics influencing total mercury in sediments (THg-S) across hydrological phases in the upper Caquetá River basin. In E1, the P10 sample (CSJR2; 7.60 µg/kg) was dominated by quartz (69.8%), exhibited low organic matter (1.38%), and consisted of coarse, angular particles with poor aggregation. These features suggest limited surface area for THg-S adsorption, consistent with the low mercury concentration observed.

Conversely, the P90 sample in E1 (PTL1; 30.54 µg/kg) had elevated Al_2O_3 and organic matter (3.40%), and SEM images (Figure 6) showed fine particles adhering to larger surfaces. Although quartz-plagioclase remained dominant, the increased presence of Al-, Fe-, and organic matter-bearing phases indicated enhanced THg-S retention. This supports the established role of clays, metallic oxides, and organic matter as key mercury sorbents in sediments.

During E2, the P10 sample (CSJR2; 26.40 µg/kg) incorporated new mineral phases such as anorthite and fraipontite, with SEM revealing particle fragmentation and diatoms. The arrival of fine material during the dry season likely contributed to increased THg-S, despite the sediment's continued siliceous character. This suggests that mineralogical changes, deposition of fine particles, and greater availability of retention surfaces during low water levels, rather than grain texture alone, explain the THg-S increase.

The P90 sample in E2 (PTR3; 162.90 µg/kg) exhibited the highest Al_2O_3 (18.1%), Fe_2O_3 (9.15%), and organic matter (3.19%), along with fine, cohesive, highly aggregated microstructures. This composition created optimal conditions for THg-S retention by forming organomineral aggregates and sorption sites, concentrating mercury in sediments with lower hydraulic energy.

These findings, illustrated in Figures 5 and 6 through SEM and XRD data, demonstrate that mercury accumulation is closely tied to mineralogical shifts, organic and metallic content, and microstructural properties, rather than sediment texture alone.

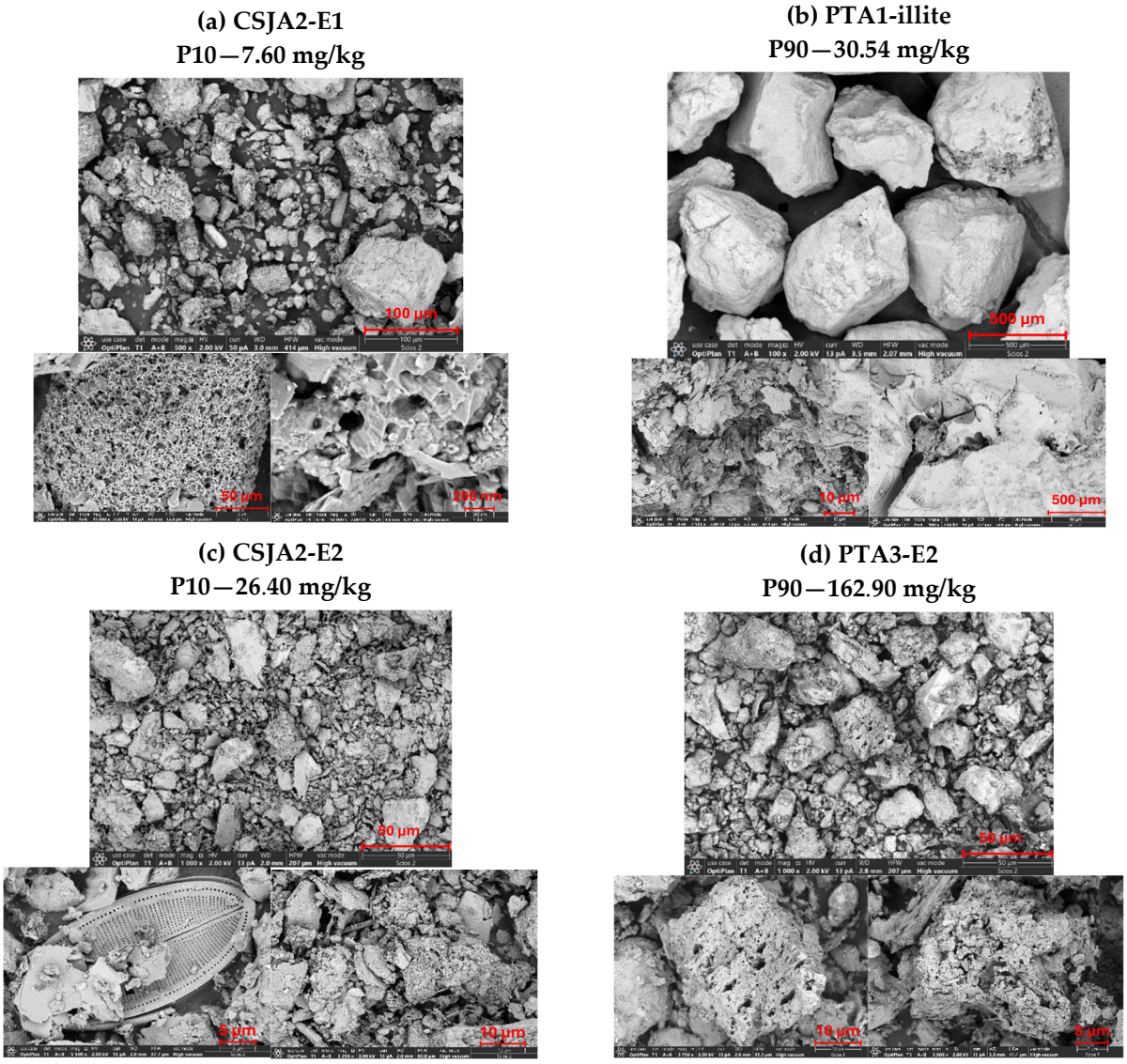


Figure 6. SEM images of representative sediment samples from the lower and upper total-mercury percentiles in E1 and E2. Panels: (**a**) CSJR2-E1 P10, (**b**) PTL1-E1 P90, (**c**) CSJR2-E2 P10, and (**d**) PTR3-E2 P90. Include scale bars, magnification, and analytical conditions in each panel.

3.4. Total Mercury in Fish and Trophic Bioaccumulation

THg in fish muscle ranged from 58.8 to 4324.5 µg/kg dry weight. Using a mean muscle moisture content of 78% (dry-to-wet weight conversion factor = 4.545), 12 individuals (9.8%) exceeded 0.5 mg/kg wet weight (Table 4). This percentage should be interpreted cautiously because Colombian Resolution 122 of 2012 establishes 0.5 mg/kg for non-predatory fish and 1.0 mg/kg for predatory fish [32].. Two omnivorous *Pimelodus blochii* individuals exceeded 0.5 mg/kg wet weight (0.569 and 0.550 mg/kg), whereas the

maximum concentration among predatory fish—0.951 mg/kg in *Pseudoplatystoma fasciatum*—approached but did not exceed the 1.0 mg/kg limit for predatory fish. Other predators of commercial or cultural importance had concentrations between 0.52 and 0.79 mg/kg wet weight. Thus, the data indicate a concern regarding dietary exposure, but regulatory compliance must be assessed according to the category of each species rather than by uniformly applying the 0.5 mg/kg value.

Table 4. Total mercury concentrations in fish muscle tissue by hydrological phase and sampling site. Values expressed in μg/kg dry weight. SD: standard deviation; CV: coefficient of variation. * La Rastra: reference site.

Hydrological Phase	Sampling Site	n	Mean ± SD	Min	Max	CV (%)
E1	El Conquistador	10	1194.80 ± 1354.04	282.10	4324.50	113.33
	La Rastra *	19	527.15 ± 333.56	58.80	1311.00	63.27
	Peñas Blancas	47	750.84 ± 647.57	156.70	2999.50	86.25
	Peterrumbe	12	717.43 ± 708.48	316.40	2904.50	98.75
E2	El Conquistador	6	1599.97 ± 1464.38	203.50	3584.00	91.53
	La Rastra *	25	983.22 ± 891.05	186.97	3374.64	90.63
	Peñas Blancas	2	646.73 ± 58.30	605.50	687.95	9.02
	Peterrumbe	2	1935.75 ± 1696.00	736.50	3135.00	87.62

The ANOVA model identified a significant effect of hydrological phase on THg in fish ($F = 5.81$; $p = 0.0175$), with higher concentrations in E2. The site effect did not reach $\alpha = 0.05$ ($F = 2.51$; $p = 0.0619$), and the interaction was also not significant (Table 4). Consequently, the higher adjusted means at El Conquistador and Peterrumbe should be regarded as trends rather than significant between-site differences. Fish mobility, species composition, trophic position, and individual size may attenuate local spatial contrasts, especially when catches differ among site-phase combinations.

Trophic guild was strongly associated with THg in fish (Spearman $r = 0.62$; $p < 0.0001$; $n = 123$), and the Kruskal–Wallis test confirmed differences among guilds ($H = 50.72$; $p < 0.0001$). Median concentrations were 380.75 μg/kg dry weight for detritivores, 468.25 μg/kg for omnivores, 1453.14 μg/kg for carnivores, and 1028.00 μg/kg for piscivores (Figure 7). Post hoc comparisons grouped detritivores and omnivores together and carnivores and piscivores together. This pattern is consistent with trophic bioaccumulation and biomagnification documented in Amazonian food webs [5,10,24]. Body mass was also positively correlated with THg ($r = 0.28$; $p = 0.0016$; $n = 122$), although trophic guild showed the clearest biological gradient.

3.5. Fish Diversity and Compositional Turnover

Fish community dynamics revealed marked differences between the reference site and those impacted by mining. La Rastra exhibited the highest richness and diversity across both hydrological phases (E_1: $S = 15$, $H' \approx 2.62$; E_2: $S = 18$, $H' = 2.73$), standing out as the only site where species richness increased. In contrast, from E_1 to E_2, richness declined drastically at mining-impacted sites: by 50% in El Conquistador, 67% in Peterrumbe, and 85% in Peñas Blancas, with captures in the latter two dropping to just two individuals during E_2. This sharp decline coincided with elevated abiotic mercury levels during the low-water period. In terms of composition, mining-impacted sites converged toward increasingly similar communities, particularly during low water whereas La Rastra maintained distinct communities in both phases, confirming that compositional similarity depends on the degree of disturbance and hydrological phase rather than geographic proximity. Although Amazonian fish communities naturally fluctuate due to hydrological connectivity, migration, habitat availability, and

opportunistic sampling [7,19,33,34], these patterns demonstrate that the reference site retains a natural fish dynamic that disturbed sites have lost to a confluence of stressors: mining pressure, reduced connectivity, sediment accumulation, and biological exposure to pollutants.

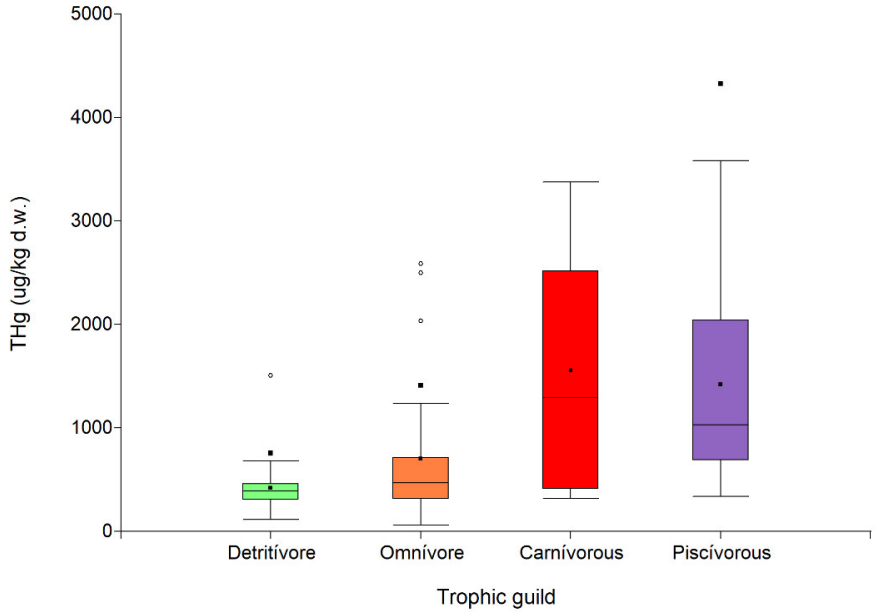


Figure 7. Boxplots of THg in fish muscle (µg/kg dry weight) for trophic guilds.

Jaccard similarity was low across the 28 site-phase comparisons (mean J = 0.071), and 11 comparisons (39.3%) had J = 0. These zero-similarity comparisons included E1 versus E2 at El Conquistador, Peñas Blancas, and Peterrumbe, indicating complete turnover of the captured species between phases. Ward clustering based on Jaccard dissimilarity produced mixed groups without strict separation by site or phase; the cophenetic correlation was 0.700 (Figure 8). This pattern is consistent with high natural temporal turnover and unequal catch representativeness and should not be interpreted as a signal attributable exclusively to mining.

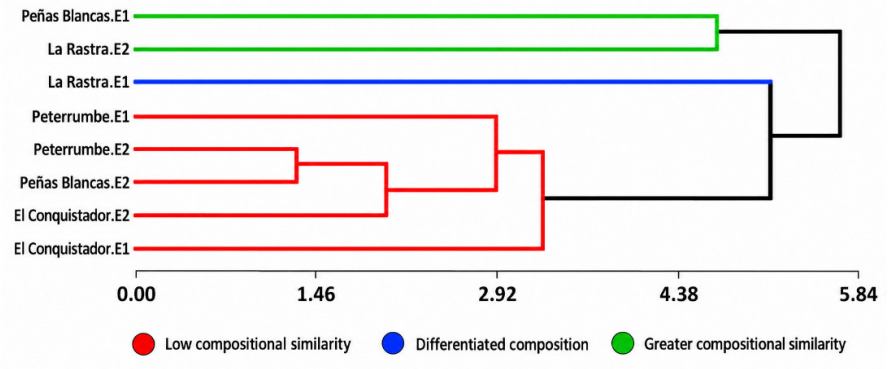


Figure 8. Hierarchical clustering of site-phase units based on Jaccard dissimilarity and Ward's method (cophenetic r = 0.700).

3.6. Integrated Relationships Among Water, Sediments, and Fish

The integrated PCA included the four sites with complete information for all three matrices in both phases (n = 8 site-phase units) (Figure 9). PC1 and PC2 explained 30.1% and 23.9% of the variance, respectively (54.0% cumulative). THg in water projected with total and suspended solids, turbidity, chloride, pH, and conductivity, reflecting the

importance of transport in the water column. Sediment THg projected with organic carbon, organic matter, conductivity, orthophosphate, and BOD_5, whereas fish THg projected with organic carbon and organic matter variables and remained separated from the main water-column gradient. The distinct vector directions show that each compartment integrates processes operating at different temporal scales.

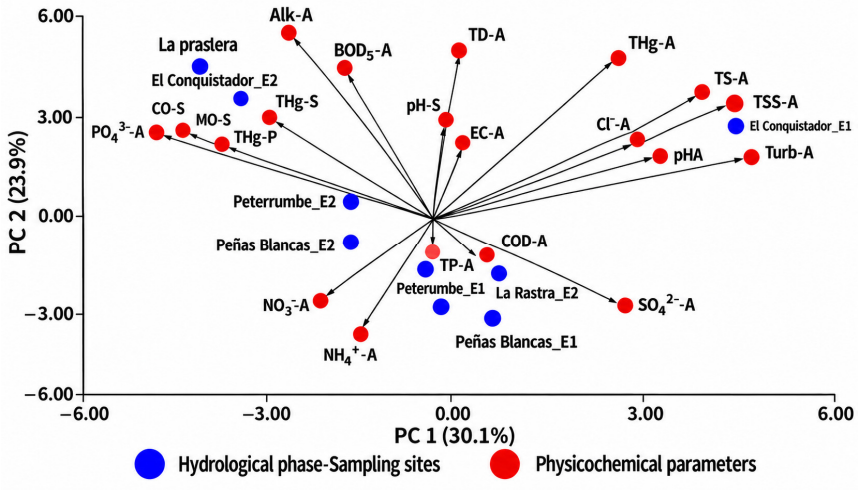


Figure 9. Integrated PCA biplot combining total mercury in water, sediment, and fish with water- and sediment-quality variables at four sites and two hydrological phases.

Correlations among matrices (water, sediments and fish) confirmed this compartmental separation. THg in water and sediments was positively associated (ϱ = 0.60; p = 0.01), whereas THg in water and fish was not correlated (ϱ = 0.07; p = 0.81), and THg in sediments and fish was also not correlated (ϱ = 0.04; p = 0.86). The previously reported r = 0.86 value for the sediment–fish relationship was incorrect. Therefore, total Hg in fish cannot be predicted directly from concurrent total concentrations in water or sediment. Biological exposure depends on species ecology and the bioavailable Hg fraction, particularly methylmercury, which was not quantified in this study.

El Conquistador during E1 appeared as an extreme site-phase unit associated with high THg in water, total suspended solids, and turbidity, consistent with the active sediment disturbance observed during sampling. La Rastra occupied a distinct region of the ordination in both phases, reflecting its particular hydrochemical and mineral-phase baseline rather than a complete absence of Hg. The integrated analysis supports basin-scale monitoring: a reference site may experience lower local mining pressure and still receive Hg through basin transport, atmospheric deposition, or integration into the food web.

4. Discussion

The distribution of total mercury in the water column of the upper Caquetá River basin reflects the combined influence of hydrological variability and local physicochemical conditions, highlighting the dynamic interactions that regulate Hg mobility and transport in tropical fluvial systems. Rather than following a uniform seasonal pattern, the relationships between THg concentrations and water-quality parameters changed between high-water and low-water conditions, suggesting shifts in the processes controlling mercury partitioning and mobilization. In particular, the contrasting associations observed with suspended solids, turbidity, organic-matter-related parameters, and dissolved ionic constituents indicate that both particulate transport and hydrochemical conditions contribute to mercury dynamics, although their

relative importance varies with hydrological phase. These findings provide evidence that understanding Hg contamination in mining-affected Amazonian rivers requires considering not only its concentrations in the water column but also the physicochemical characteristics that influence its environmental distribution, persistence, and potential transfer to other aquatic compartments.

The ANOVA of physicochemical parameters and mercury levels was used to evaluate effect of hydrological phases, sampling sites and its interaction (Table A1). For pH, a highly significant effect of hydrological phase ($F = 56.00$; $p < 0.0001$), sampling site ($p = 0.0328$), and their interaction ($p < 0.0001$) was demonstrated, with higher values during high water (E1 = 6.98) than during low water (E2 = 6.36), suggesting that the more acidic conditions in E2 may favor mercury methylation and bioavailability. La Rastra, the reference site without mining activity, differed significantly from the other sites, with the lowest pH (6.19), lowest electrical conductivity (19.50 μS/cm), and lowest alkalinity (11.00 mg/L $CaCO_3$), reflecting a low ionic load consistent with the absence of direct anthropogenic disturbance [14].

The organic load, represented by BOD_5 ($F = 32.93$; $p < 0.0001$), was significantly higher during low water (BOD_5 = 6.73 mg/L) than during high water (BOD_5 = 2.94 mg/L), indicating an accumulation of dissolved organic matter under lower-discharge conditions that favors mercury complexation and retention in more bioavailable forms [27,35].

Electrical conductivity and alkalinity did not differ between phases ($p > 0.05$), but did differ among sampling sites (EC: $F = 5.02$, $p = 0.0006$; alkalinity: $F = 11.66$, $p < 0.0001$), evidencing spatial control of ionic composition associated with local geochemical factors. Variables such as turbidity, TSS, and TS did not show significant differences ($p > 0.05$), although their high variability suggests intermittent sediment-resuspension processes, which are relevant given that 20–95% of fluvial mercury is associated with the particulate fraction [35]. Nevertheless, La Rastra recorded high turbidity (73.38 NTU) comparable to that of sites with active dredging, confirming that the natural dynamics of the river generate particulate-material transport independently of mining activity [19].

Overall, the hydrological phase regulates organic load and pH, whereas spatial variability controls ionic composition, resulting in a dilution effect during E1 and a concentration effect during low water, a pattern consistent with that reported for Amazonian systems [36] and Colombian watersheds impacted by artisanal gold mining [37]. La Rastra, with the lowest concentrations of THg in water (0.84 ± 0.26 μg/L) and the lowest ionic-load values, constitutes a geochemical baseline that allows the contribution of mining-derived mercury to be distinguished from the natural behavior of the fluvial system.

Comparison of the two hydrological phases reveals a clear change in the covariation between THg-A and the physicochemical parameters of the water. During high water, THg-A was primarily associated with TSS-A, TS-A, Turb-A, and BOD_5-A, suggesting a transport mechanism dominated by suspended particulate and organic material. During low water, in contrast, THg-A became decoupled from the solid particles variables and approached the NH_4-A sector, suggesting a greater influence of local hydrochemical conditions.

The results indicate that mercury dynamics in the Caquetá River do not follow a single transport mechanism. During high-water periods, the physical transport of particles appears to be more significant, whereas during low-water periods, other factors—potentially linked to local hydrochemical conditions—become relevant.

An "apparent Hg/TSS ratio" has been determined as an exploratory measure. While this ratio helps illustrate such differences, it does not, in itself, constitute evidence of a greater partitioning of mercury into the solid phase. The apparent Hg/TSS ratio was additionally examined to explore the relationship between total mercury concentrations

in water and suspended-particle abundance. The median ratio increased from 31.54 mg/kg during the high-water phase (E1) to 78.00 mg/kg during the low-water phase (E2), representing an approximately 2.47-fold increase. This pattern suggests that, during low-water conditions, total mercury concentrations were relatively higher in relation to the TSS load. Conversely, during high-water conditions, greater particulate transport may have contributed to lower Hg/TSS ratios through the mobilization of larger amounts of suspended material. These contrasting patterns are consistent with the seasonal variability observed in the multivariate analysis and suggest that mercury dynamics cannot be explained solely by suspended-solids abundance. Nevertheless, this ratio represents an apparent Hg-to-solids relationship rather than a direct measurement of particulate-bound mercury, since THg was determined in unfiltered water samples and therefore includes both dissolved and particulate fractions.

In the same way, the PCA confirmed that the distribution of THg-A in the upper Caquetá River basin was modulated by the hydrological phase. In E1, the pattern was dominated by physical particle transport, with El Conquistador strongly associated with the THg-A–solids–turbidity gradient. In E2, THg-A separated from the TSS gradient and was related to a different set of hydrochemical conditions, close to NH_4^+-A and the Peterrumbe and Peñas Blancas sites. These results indicate that total mercury in water did not exhibit uniform behavior across phases, but rather responded to seasonal changes in hydraulic energy, particulate load, and local conditions at each site.

The correlation between THg-S and water-quality parameters, including THg-A, is shown in Figure 2b. Sediment THg (THg-S) was positively correlated with THg-A ($p < 0.001$), evidencing a direct association between the water and sediment matrices. This result indicates that sediment actively participates in mercury accumulation, exchange, and redistribution processes rather than acting solely as a passive reservoir. In water, Hg can be transported in dissolved or colloidal form or associated with suspended particles, and subsequently incorporated by sedimentation, adsorption, or coprecipitation with mineral and organic phases. This dynamic has been described in water–suspended-material–sediment systems and is consistent with recent studies in Amazonian environments impacted by gold mining, where sediment functions as a key compartment for Hg storage and transfer to the food web [24,38].

Likewise, the positive correlation between THg-S and BOD_5-A ($p < 0.001$) reinforces the role of organic matter in water–sediment transfer. A higher organic load in the water column may promote the transport of Hg bound to organic complexes, colloids, or fine particles, as well as its subsequent retention in sediments with adsorption capacity. This result consists of the high affinity of mercury for reduced functional groups in organic matter, particularly sulfur-containing groups, and with its tendency to associate with fine, organic, and mineralogically reactive sediment phases [26,31,38].

THg-S showed significant negative correlations with water-quality parameters such as pH ($p < 0.001$), TS ($p < 0.001$), alkalinity ($p = 0.01$), Cl^- ($p< 0.001$), SO_4^{2-} ($p< 0.001$), and NH_4^+ ($p < 0.001$). These associations indicate that THg-S accumulation was related to hydrochemical conditions such as lower pH values and lower concentrations of some ions. In environmental terms, the combined interaction of parameters such as pH, organic matter, suspended particles, redox conditions, and mineral phases can modify mercury speciation, its competition for adsorption sites, its complexation with dissolved ligands, and its redistribution among aqueous, particulate, and sedimentary phases [28,29].

Sediment mercury concentrations indicate that, without direct mining sources, mercury primarily derives from particulate matter transported from upstream during flood events and from atmospheric deposition accumulated in floodplain soils. In contrast, at mining sites, low-water mercury concentrations are attributed to reduced flow and the direct deposition of amalgamation residues [31].

Chlorite in sediments plays a key role in natural mercury adsorption. Illite, a 2:1 clay mineral with a high specific surface area and strong negative interlayer charge, effectively retains mercury ions through electrostatic adsorption, which matches the observed high mercury levels at specific sites [39]. In contrast, kaolinite, nacrite, and halloysite—1:1 clays with no interlayer space—retain less mercury, though they can immobilize some via surface adsorption. Three polytypes of cronstedtite, an iron-rich serpentine group mineral, were also found at several sites, highlighting the presence of iron-bearing phases that interact with mercury. Overall, mercury retention capacity in sediments varies across the basin, depending on local mineralogy and lithology [14].

Total mercury in sediments (THg) varied significantly by hydrological phase, sampling site, and their interaction, showing that mercury dynamics are influenced by both time and location. Mercury concentrations were higher during low water (88.36 μg/kg) than during high water (30.96 μg/kg), likely because reduced flow facilitated the deposition of mercury-rich particles from amalgamation activities. Among the sites, Peterrumbe had the highest concentrations (101.86 μg/kg), followed by Peñas Blancas (77.62 μg/kg) and El Conquistador (67.26 μg/kg). La Pradera had the lowest value (29.86 μg/kg). At the same time, La Rastra, a reference site with no mining, displayed intermediate levels (40.28 μg/kg) and an inverse seasonal pattern, with more mercury during high water than low water. This suggests that, without direct mining, mercury in sediments is mainly delivered by upstream transport during floods or by atmospheric deposition during the rainy season [40].

Sediment chemistry did not differ significantly between hydrological phases but did vary among sites. Notably, Peterrumbe had a lower pH (5.30), which may increase mercury desorption and its bioavailability in the water. Organic carbon, organic matter, and conductivity were temporally stable. Still, a trend towards higher organic matter during low water (3.21%) may favor the reducing conditions that promote mercury methylation at the sediment-water interface. X-ray diffraction analysis showed a negative correlation between total mercury and silica (SiO_2), and an association with quartz. This suggests a dilution effect: as quartz increases, components with higher adsorption capacity (like organic matter, clays, and metal oxides) decrease, making quartz an indicator of less reactive sediments. These findings underscore the importance of reactive mineral phases in mercury retention, rather than inert minerals like quartz [26,38].

Quartz content varied significantly between sites, with La Rastra showing the lowest value (22.11%), distinct from other locations. This mineralogical composition, alongside higher Fe_2O_3 (11.75%) and Al_2O_3 (20.08%) levels, indicates a lithology dominated by iron and aluminum oxyhydroxides with mercury adsorption capacity. In contrast, sediments from disturbed sites are mainly quartz due to dredging operations.

X-ray fluorescence (XRF) analysis revealed that THg-S is positively correlated with aluminum, iron, and manganese oxides in sediments, suggesting these reactive phases enhance THg accumulation. The oxides, oxyhydroxides, and amorphous or weakly crystalline forms of Fe, Al, and Mn are important geochemically due to their high surface area and metal-retention capacity. Consequently, sediments rich in these phases serve as more effective THg reservoirs [8,31,38].

However, this retention does not imply permanent immobilization. Under changes in redox potential, organic matter content, or hydrological dynamics, iron and manganese oxides can transform or undergo reductive dissolution, releasing previously retained Hg and increasing its availability for microbial processes, including methylation. In this sense, the positive association between THg-S and metal oxides should be interpreted as evidence of dynamic geochemical accumulation, where the sediment can function both as a temporary sink and as a secondary source of mercury under specific environmental conditions [8,31,38]. THg-S shows positive correlations with Al_2O_3, Fe_2O_3, MnO, Al, and

Fe, indicating that oxides and hydroxides of Fe, Al, and Mn are key for mercury retention in sediments. Quartz (SiO_2) displays a negative correlation, suggesting that higher quartz content dilutes sorption sites for THg adsorption. In the upper Caquetá River basin, mercury dynamics are controlled by physicochemical, hydrological, and mineralogical factors. Organic matter, pH, and ion composition influence THg in the water, while reactive minerals and organic matter drive retention in sediments. This demonstrates environmental coupling among water, sediment, and mercury in a mining-impacted Amazonian system [8,24,31].

Multivariate analysis (PCA) revealed seasonal and geochemical controls on total mercury distribution in sediment (THg-S). During the high-water phase (E1), THg-S was predominantly associated with reactive mineral phases—specifically clay content and oxides/hydroxides of Fe, Al, and Mn (Al_2O_3, Fe_2O_3, MnO)—which enhance metal retention via adsorption and complexation. The reference site, La Rastra, positioned consistently along positive PC1, exhibited this reactive mineralogical signature. Conversely, mining-affected sites such as Calle San Juan, Fidelicias, La Pradera, and Puerto Príncipe grouped with sand, quartz, and SiO_2, reflecting a mineralogical dilution effect where coarse, siliceous material provides fewer reactive binding sites for immobilization.

During the low-water phase (E2), a clear hydrological shift occurred: THg-S decoupled from Fe and Al oxides and became strongly associated with organic matter (MO-S, CO-S) and fine clay fractions. Lower flow rates and longer water residence times in low-energy environments (such as Peterrumbe and Peñas Blancas) favored the deposition and accumulation of fine, organic-rich sediments that form stable organo-mineral complexes with mercury. Overall, these findings demonstrate that sediment mercury retention in the upper Caquetá River basin shifts dynamically between mineralogical control during high-water flow and organo-mineral control under low-water conditions.

The reference site La Rastra, positioned toward the positive end of CP1 in both hydrological phases and consistently associated with Fe_2O_3, Al_2O_3, Al, and other reactive mineral phases, maintains a distinct mineralogical signature compared to sites affected by mining activity. This distinction likely reflects the background geochemical characteristics of the Orteguaza River system, without direct influence from alluvial gold dredging. In contrast, the separation of several mining sites from La Rastra along CP1 represents a gradient of geochemical differentiation in the sediment, potentially resulting from removal, washing, and redistribution of fine fractions during dredging operations. This pattern suggests that mining activity may alter the relative proportion of reactive fine phases compared to sandy or siliceous fractions, thereby modifying the sediment's potential THg-S retention capacity.

The seasonal decoupling observed between abiotic and biotic matrices in the upper Caquetá River basin represents a core phenomenon for understanding total mercury THg dynamics within the system. While THg-S concentrations peaked during the high-water seasonal pattern consistent with the transport and deposition of fine particulate matter carried from upper reaches during peak flows the ichthyofauna exhibited an inverse response. In fish muscle tissue, THg levels increased significantly during the low-water season across both mined sectors and unimpacted reaches; for instance, at the reference site (La Rastra), mean muscle concentrations rose from high-water baselines to marked peaks during low water. This seasonal accumulation stems from the severe contraction of available aquatic habitats during low water, which confines organisms to reduced water volumes and heightens their exposure to methylated mercury in the water column, thereby promoting bioaccumulation regardless of proximity to point source mining activities [6–8,36]. The lack of spatial significance in fish muscle variation suggests that intrinsic biological drivers such as trophic position, body size, and feeding habits exert a

predominant control that masks local geochemical differences. Consequently, contaminant transfer intensifies sharply along the food web, accumulating the highest THg burdens in carnivorous and piscivorous guilds. This behavior was striking in high-trophic-level species of commercial and subsistence value, including the *Pseudoplatystoma fasciatum*, *P. punctifer*, *Hydrolycus scomberoides*, *Ageneiosus inermis* and *Calophysus macropterus*. The similarity in mercury levels between piscivores and carnivores supports convergent loading across upper trophic levels, while the positive correlation between body weight and muscle THg concentrations ($r = 0.28$; $p = 0.0016$; $n = 122$) confirms progressive ontogenetic bioaccumulation throughout the fish life cycle [10].

The ecotoxicological and public health implications of this trophic and seasonal magnification are critical, as 9.8% of sampled fish (n = 123) exceeded the maximum permissible human consumption limit of 500 µg/kg w.w. established by Resolution 122 of 2012 [1] calculated from dry weight determinations using a reference muscle moisture factor of 78%. This exposure risk is strongly localized in space and time: at El Conquistador and Peterrumbe during low water periods, coinciding with peak artisanal alluvial dredging intensity, over 50% of captured individuals breached this regulatory threshold. This trend aligns with downstream observations at the Puerto Zábalo indigenous community in Los Monos, where over 50% of sampled fish exceeded safety limits, demonstrating that risk assessments relying on basin-wide averages systematically underestimate real exposure for riparian and indigenous populations reliant on large, high trophiclevel prey [24,41,42].

Concurrently with bioaccumulation, mercury contamination interacts directly with fish community structure. During low water, mining-impacted sites experienced severe reductions in species richness with losses of 50% at El Conquistador, 85% at Peñas Blancas, and 67% at Peterrumbe which coincided directly with peak abiotic THg levels. This evidences that biodiversity loss is driven not merely by physical habitat alteration from dredging, but also by acute toxic stress exerted by mercury in the water column [43], threatening the integrity of key refuge networks such as the Peregrinos lagoon complex.

Ultimately, this joint action of physical habitat degradation and chemical stress resulted in a quantitative restructuring of fish assemblages, as demonstrated by Jaccard similarity indices near zero across most inter-site comparisons. This pattern reflects a nearly complete compositional turnover (β-diversity), disrupting the longitudinal connectivity expected in undisturbed river systems. Hierarchical cluster analysis confirmed that site affinity was governed by disturbance intensity and hydrological phase rather than geographic proximity; while mined sites underwent marked biotic homogenization during low water, the reference site (La Rastra) remained a distinct, isolated cluster across both hydrological phases. Together, these findings confirm that the synergy between alluvial dredging and low water dismantles functional river connectivity and establishes effective ecological barriers, restructuring fish communities at a basin-wide scale [40,44].

5. Conclusions

Total mercury showed compartment-specific behavior in the upper Caquetá River basin. THg concentrations in water were highly variable and frequently exceeded screening criteria, but site and hydrological-phase effects were not statistically significant after accounting for variance heterogeneity. Sediments provided the clearest spatiotemporal signal: concentrations increased during low-water conditions at mining-affected sites and were associated with fine particles, organic matter, and reactive Fe, Al, and Mn phases. Fish integrated exposure over longer time scales; hydrological phase and trophic guild were more informative than sampling site, and carnivorous and piscivorous guilds had the highest concentrations.

https://doi.org/10.3390/environments13120643

THg in water and sediments covaried, whereas neither abiotic matrix predicted THg in fish. This decoupling demonstrates that total-mercury measurements do not substitute for determinations of methylmercury or bioavailability. Future mercury monitoring should prioritize accumulation in sediments during low-water conditions, predatory fish and those frequently consumed, as well as periodic basin-wide sampling that maintains La Rastra as a reference site while simultaneously expanding coverage downstream. Species-specific regulatory limits should be applied when interpreting fish safety, and future studies should quantify methylmercury and biomarkers of human exposure.

The ability of sediments to retain mercury is largely determined by their mineral composition. Chlorite and illite, due to their specific structure and electrostatic charge, exhibit the highest mercury retention. In contrast, minerals such as kaolinite, nacrite, and halloysite retain much lower concentrations of mercury, as they lack interlayer spaces between their layers. In minerals containing iron phases, these iron components interact with mercury.

The main findings show that Hg in water was highly variable and frequently exceeded quality criteria; sediments accumulated Hg more strongly during low-water conditions at mining-affected sites; and Hg in fish was explained more consistently by hydrological phase and trophic guild than by sampling site. These results establish a baseline for basin-scale environmental and public-health monitoring.

Author Contributions: S.K.G.-E.: Conceptualization, Data curation, Formal analysis, Investigation, Methodology, Visualization, Writing—original draft. L.M.-L.: Conceptualization, Writing—original draft, Funding acquisition, Project administration, Resources, Supervision, Writing—review and editing. N.F.N.-G.: Investigation (XRD and XRF analyses), Methodology, Mineralogical and geochemical interpretation, Writing—review and editing. M.S.C.-G.: Methodology (biotic component), Investigation, Writing—review and editing. C.J.-P.: Methodology, Mineralogical and geochemical interpretation, Writing—review and editing. F.C.: Statistics analysis, writing, review and editing. All authors have read and agreed to the published version of the manuscript.

Funding: The authors from the Universidad de la Amazonia and the Universidad del Tolima acknowledge the financial support provided by the project "Análisis del impacto socio ambiental del mercurio y tecnologías sostenibles para su remoción en la cuenca alta del Rio Caquetá. Caquetá-Putumayo" (BPIN-2022000100050), through Minciencias/SGR resources.

Data Availability Statement: Before publication, requests for data access may be directed to the corresponding author.

Acknowledgments: The authors thank the riverine communities for their collaboration, and the local fishers, whose knowledge and field support were essential to the sampling program. During the preparation of this manuscript/study, the author Lis Manrique-Losada used ChatGPT basado en el modelo GPT-6, desarrollado por OpenAI (generative AI) to reconstruct figures, create a graphical abstract, as a supporting tool for the review and editing of the scientific text. and assist in generating and translating text into English. The authors have reviewed and edited the output and take full responsibility for the content of this publication.

Conflicts of Interest: The authors declare no conflict of interest.

Abbreviations

The following abbreviations are used in this manuscript:

EC-A	Electrical conductivity in water matrix
Turb-A	Turbidity in water matrix
TSS-A	Total suspended solids in water matrix
TS-A	Total solids in water matrix

TH-A	Total hardness in water matrix
Alk-A	Alkalinity in water matrix
BOD_5-A	Biochemical oxygen demand in water matrix
COD-A	Chemical oxygen demand in water matrix
TP-A	Total phosphorus in water matrix
E1	High water phase
E2	Low water phase
THg-A	Total mercury in water matrix
THg-S	Total mercury in sediments matrix
ASGM	Artisanal and small-scale gold mining

Appendix A

Table A1. Physicochemical parameters analyzed in water samples according to *Standard Methods for the Examination of Water and Wastewater* [17].

Parameter	Method	Unit
Total alkalinity	SM 2320 B	mg/L as $CaCO_3$
Residual aluminum	SM 3500-Al B	mg/L as Al^{3+}
Chlorides	SM 4500-Cl-B	mg/L Cl^-
Electrical conductivity	SM 2510 B	µS/cm
Total hardness	SM 2340 C	mg/L $CaCO_3$
Phosphates	SM 4500-P C	mg/L PO_4^{3-}
Total iron	SM 3500-Fe B	mg/L
Nitrates	SM 4500-NO_3^- B	mg/L NO_3^-
Ammoniacal nitrogen	SM 4500-NH_3 C	mg/L NH_3-N
pH	SM 4500-H^+ B	pH units
Sulfates	SM 4500-SO_4^{2-}	mg/L SO_4^{2-}
Turbidity	SM 2130 B	NTU
Total suspended solids	SM 2540 D	mg/L
Total dissolved solids	SM 2540 C	mg/L
Total solids	SM 2540 B	mg/L
Biochemical oxygen demand (BOD_5)	SM 5210 B	mg/L
Chemical oxygen demand (COD)	SM 5220 D	mg/L O_2
Total mercury	EPA 7473	µg/L

https://doi.org/10.3390/environments13120643

Table A2. Water Quality parameters of the upper Caquetá river basin.

Hydrologic Phase	Sampling Site	pH-A		EC-A (µS/cm)		Turb-A (NTU)		TSS-A (mg/L)		TS-A (mg/L)		BOD_5-A (mg/L)		Alk-A (mg/L)		TD-A (mg/L)		Cl^--A (mg/L)		SO_4^{2-}-A (mg/L)		NH_4^+-A (mg/L)		NO_3^--A (mg/L)		PO_4^{3-}-A (mg/L)		TP-A (mg/L)		THg A (µg/L)		Apparent Hg/TSS Ratio (mg/kg)	
		Average	SD	Average	SD	Average	SD	Average	SD	Average	SD	Average	SD	Average	SD	Average	SD	Average	SD	Average	SD	Average	SD	Average	SD	Average	SD	Average	SD	Average	SD	Average	SD
E1	Peñas Blancas	6.85	0.33	23.06	8.30	13.84	14.80	17.65	4.73	54.83	18.99	2.30	1.99	17.47	6.87	25.96	14.85	111.05	42.02	5.11	2.79	3.37	0.68	1.70	0.83	0.04	0.03	0.40	0.33	0.43	0.05	25.85	7.15
	Puerto Príncipe	7.07	0.03	21.53	0.17	12.40	0.80	22.83	13.14	201.58	41.72	2.00	0.00	32.36	9.01	41.22	8.50	139.23	8.55	9.33	0.32	2.92	0.31	1.29	0.26	0.05	0.01	0.61	0.06	0.54	0.20	29.58	17.73
	Peterrumbe	7.25	0.37	27.09	3.53	18.60	9.91	26.60	12.22	122.55	50.76	3.30	2.39	23.35	7.45	36.31	7.91	118.30	37.12	8.91	3.63	2.30	0.35	1.66	0.83	0.04	0.01	0.41	0.33	0.88	0.48	44.83	38.30
	Fidelicias	7.33	0.10	57.50	15.38	39.36	5.97	20.25	6.43	232.77	87.36	2.00	1.00	50.70	9.48	36.66	22.25	78.79	11.72	9.50	1.70	0.97	0.14	2.39	0.76	0.10	0.02	0.24	0.06	1.07	0.58	61.70	49.38
	El Conquistador	7.48	0.29	53.50	11.80	29.13	15.80	39.19	18.38	254.31	48.13	5.13	4.55	35.08	19.15	35.56	3.71	108.92	25.04	7.76	4.28	0.47	0.12	0.75	0.56	0.04	0.04	0.15	0.16	5.56	1.19	170.26	92.81
	Calle San Juan	7.14	0.49	58.19	13.70	9.90	6.63	16.50	1.06	120.75	20.51	3.25	0.35	50.16	13.73	36.86	0.29	90.93	5.11	8.51	0.57	0.91	0.42	1.00	1.42	0.07	0.02	0.18	0.07	0.81	0.56	47.80	30.78
	La Pradera	7.24	0.10	59.60	10.51	11.19	3.02	13.76	4.74	121.51	18.40	3.00	3.46	52.31	4.67	34.76	2.23	89.54	23.23	7.04	5.35	1.32	0.08	2.61	4.52	0.17	0.18	0.32	0.14	0.41	0.00	32.10	10.19
	La Rastra	5.46	0.42	10.00	0.00	75.83	19.41	37.00	9.90	52.00	18.38	2.75	0.35	9.00	2.83	12.00	5.66	46.18	1.24	2.70	1.32	1.42	0.44	3.11	0.14	0.00	0.00	0.02	0.02	0.92	0.01	25.67	7.06
E2	La Pradera	6.23	0.13	56.49	6.52	10.37	0.73	28.67	14.05	73.00	19.11	3.67	0.76	29.44	4.41	25.56	2.42	38.50	7.23	5.99	0.96	0.79	0.11	1.74	0.81	0.05	0.01	0.19	0.01	1.78	1.07	65.76	26.97
	Fidelicias	6.48	0.07	117.04	30.63	13.38	2.55	16.00	7.81	149.83	16.24	4.33	0.58	69.81	14.34	60.74	10.83	12.77	2.58	4.79	3.95	0.80	0.39	0.00	0.00	0.10	0.02	0.21	0.04	1.23	0.09	86.24	30.03
	El Conquistador	6.09	0.18	53.16	3.72	6.61	0.63	39.33	18.82	70.33	33.86	10.00	0.87	31.11	3.89	35.74	5.13	16.20	8.96	0.00	0.00	0.88	0.20	0.83	0.72	0.07	0.01	0.26	0.02	1.74	0.12	49.65	17.39
	Calle San Juan	6.31	0.15	53.59	9.60	6.64	3.81	22.33	21.36	71.83	7.65	7.50	3.50	30.37	6.42	27.96	3.61	36.43	7.97	5.29	0.41	1.32	0.54	0.91	1.06	0.07	0.01	0.17	0.04	0.87	0.08	63.50	39.78

Peñas Blancas	6.39	0.14	23.40	8.46	7.31	8.82	6.11	0.96	58.83	14.34	6.67	0.76	17.22	8.18	13.89	3.38	25.16	7.50	4.83	1.59	0.85	0.10	6.52	7.88	0.05	0.01	0.49	0.04	2.23	0.45	379.07	143.00
Puerto Príncipe	6.33	0.15	31.19	3.49	14.19	6.28	20.00	10.14	81.00	5.77	5.67	0.29	20.74	0.85	24.44	8.33	28.62	4.77	7.28	0.46	0.64	0.11	1.30	0.45	0.05	0.02	0.48	0.03	1.88	0.38	134.90	120.51
Peterrumbe	6.16	0.12	47.99	4.29	9.17	6.12	8.89	2.55	38.17	22.61	7.50	2.29	17.41	4.32	21.30	7.86	42.88	2.09	5.72	1.85	0.83	0.05	1.63	0.92	0.04	0.01	0.59	0.02	1.55	0.07	184.61	57.63
La Rastra	6.93	0.83	29.01	4.49	70.93	7.67	54.00	21.21	111.75	16.62	8.50	0.71	13.00	1.41	19.78	5.72	45.79	10.44	138.50	28.28	0.50	0.01	3.14	1.36	0.01	0.00	3.24	0.24	0.84	0.30	17.95	12.68

Table A3. Descriptive statistics (mean ± SD) of the geochemical properties of the sediment matrix. SD: standard deviation; EC: conductivity; CO: organic carbon; OM: organic matter; THg: total mercury. E1: high water; E2: low water study (153.15 µg/kg).

Variable	Unit	Hydrological Phase		Sampling Site							
		High Waters (n = 27)	**Low waters (n = 23)**	**Peñas Blancas (n = 8)**	**El Conquistador (n = 7)**	**Pete-umbe (n = 8)**	**La Rastra (n = 4)**	**Puerto Príncipe (n = 6)**	**Fideli-cias (n = 6)**	**Calle San Juan (n = 5)**	**La Pradera (n = 6)**
pH	Units	6.03 ± 0.571	6.22 ± 0.593	5.31 ± 0.321	6.42 ± 0.498	5.99 ± 0.529	5.91 ± 0.145	6.24 ± 0.492	6.59 ± 0.306	6.41 ± 0.614	6.30 ± 0.445
CE	mg/kg	125.30 ± 41.46	118.29 ± 49.37	105.96 ± 35.65	138.78 ± 67.96	124.65 ± 35.18	72.31 ± 44.98	129.20 ± 36.71	110.55 ± 16.70	118.23 ± 36.90	161.42 ± 43.70
CO	%	1.47 ± 1.13	1.84 ± 1.08	2.14 ± 1.06	2.10 ± 1.78	1.58 ± 0.513	1.35 ± 0.922	1.18 ± 0.571	1.92 ± 1.18	0.908 ± 0.808	1.51 ± 1.37
mes	%	2.56 ± 1.92	3.18 ± 1.86	3.68 ± 1.77	3.60 ± 3.02	2.78 ± 0.927	2.35 ± 1.61	2.07 ± 1.00	3.36 ± 2.09	1.58 ± 1.36	2.60 ± 2.37
THg	µg/kg	32.31 ± 18.53	91.15 ± 48.81	67.45 ± 46.07	64.33 ± 30.94	85.06 ± 70.20	40.29 ± 18.42	63.72 ± 44.70	51.20 ± 37.84	53.68 ± 63.55	29.86 ± 17.85
SAND	%	52.16 ± 20.63	52.44 ± 19.51	54.71 ± 14.83	40.79 ± 19.26	39.81 ± 12.60	48.56 ± 20.78	53.76 ± 20.14	52.69 ± 22.96	65.68 ± 23.11	68.56 ± 18.42
LIME	%	27.51 ± 15.39	27.60 ± 15.10	23.65 ± 10.42	37.20 ± 13.36	38.80 ± 10.20	20.50 ± 20.81	28.80 ± 14.44	26.40 ± 17.33	21.68 ± 19.15	16.00 ± 8.10
Clay	%	20.33 ± 12.13	19.96 ± 6.49	21.64 ± 9.38	22.01 ± 9.36	21.39 ± 5.06	30.94 ± 15.26	17.44 ± 6.20	20.91 ± 9.00	12.64 ± 4.38	15.44 ± 14.70

Table A4. Descriptive statistics (mean ± SD) of the mineralogical (XRD) and geochemical composition of major oxides (XRF) of the sediment matrix (n = 50) in the Caquetá River, according to hydrological phase and sampling site. SD: standard deviation; XRD: X-ray diffraction; XRF: X-ray fluorescence. E1: high water; E2: low water.

Variable	Unit	Hidrological Phase		Sampling Site							
		High water (n = 27)	**Low water (n = 23)**	**Peñas Blancas (n = 8)**	**El Conquistador (n = 7)**	**Peterrumbe (n = 8)**	**La Rastra (n = 4)**	**Puerto Príncipe (n = 6)**	**Fidelidades (n = 6)**	**Calle San Juan (n = 5)**	**La Pradera (n = 6)**
Quartz	%	55.87 ± 22.74	53.57 ± 24.54	67.91 ± 26.61	49.13 ± 26.64	54.42 ± 27.16	22.11 ± 25.39	54.75 ± 12.66	45.28 ± 12.72	67.06 ± 10.32	65.67 ± 10.27
SiO_2	%	66.18 ± 4.12	65.02 ± 4.65	70.47 ± 6.72	64.53 ± 1.19	63.65 ± 2.06	59.82 ± 3.26	65.63 ± 1.95	64.20 ± 2.17	67.92 ± 4.51	66.62 ± 1.84

Al_2O_3	%	16.60 ± 1.73	16.94 ± 1.90	16.91 ± 1.57	16.63 ± 0.911	17.68 ± 0.838	20.07 ± 1.30	16.37 ± 1.15	16.25 ± 1.23	14.96 ± 2.27	15.67 ± 1.72
Fe_2O_3	%	8.43 ± 1.89	9.42 ± 2.44	6.66 ± 2.84	9.25 ± 0.521	9.55 ± 0.900	11.75 ± 2.16	8.65 ± 1.02	10.24 ± 2.49	7.93 ± 2.26	8.32 ± 1.13
K_2O	%	2.68 ± 0.795	2.78 ± 0.567	1.68 ± 1.16	2.83 ± 0.193	2.87 ± 0.323	3.52 ± 0.315	2.84 ± 0.201	2.74 ± 0.120	3.07 ± 0.310	2.85 ± 0.147
CaO	%	2.92 ± 1.15	2.60 ± 0.761	1.57 ± 1.19	3.15 ± 0.648	2.85 ± 0.445	1.67 ± 0.048	3.17 ± 0.574	3.13 ± 0.834	3.43 ± 0.778	3.27 ± 0.903
MgO	%	1.14 ± 0.710	1.18 ± 0.677	0.668 ± 0.755	1.57 ± 0.165	1.30 ± 0.543	0.427 ± 0.104	1.36 ± 0.687	1.49 ± 0.734	0.888 ± 0.812	1.35 ± 0.687
TiO_2	%	1.20 ± 0.198	1.23 ± 0.170	1.41 ± 0.226	1.16 ± 0.067	1.22 ± 0.077	1.42 ± 0.129	1.22 ± 0.054	1.07 ± 0.086	1.07 ± 0.292	1.16 ± 0.089
P_2O_5	%	0.183 ± 0.094	0.172 ± 0.079	0.117 ± 0.101	0.184 ± 0.057	0.190 ± 0.057	0.346 ± 0.092	0.125 ± 0.034	0.208 ± 0.078	0.157 ± 0.062	0.167 ± 0.043
BaO	%	0.083 ± 0.054	0.073 ± 0.020	0.042 ± 0.032	0.080 ± 0.021	0.078 ± 0.018	0.157 ± 0.109	0.075 ± 0.0098	0.074 ± 0.0062	0.081 ± 0.0099	0.078 ± 0.0087
MnO	%	0.164 ± 0.076	0.183 ± 0.077	0.092 ± 0.070	0.178 ± 0.018	0.190 ± 0.022	0.198 ± 0.048	0.167 ± 0.017	0.272 ± 0.140	0.154 ± 0.064	0.154 ± 0.011

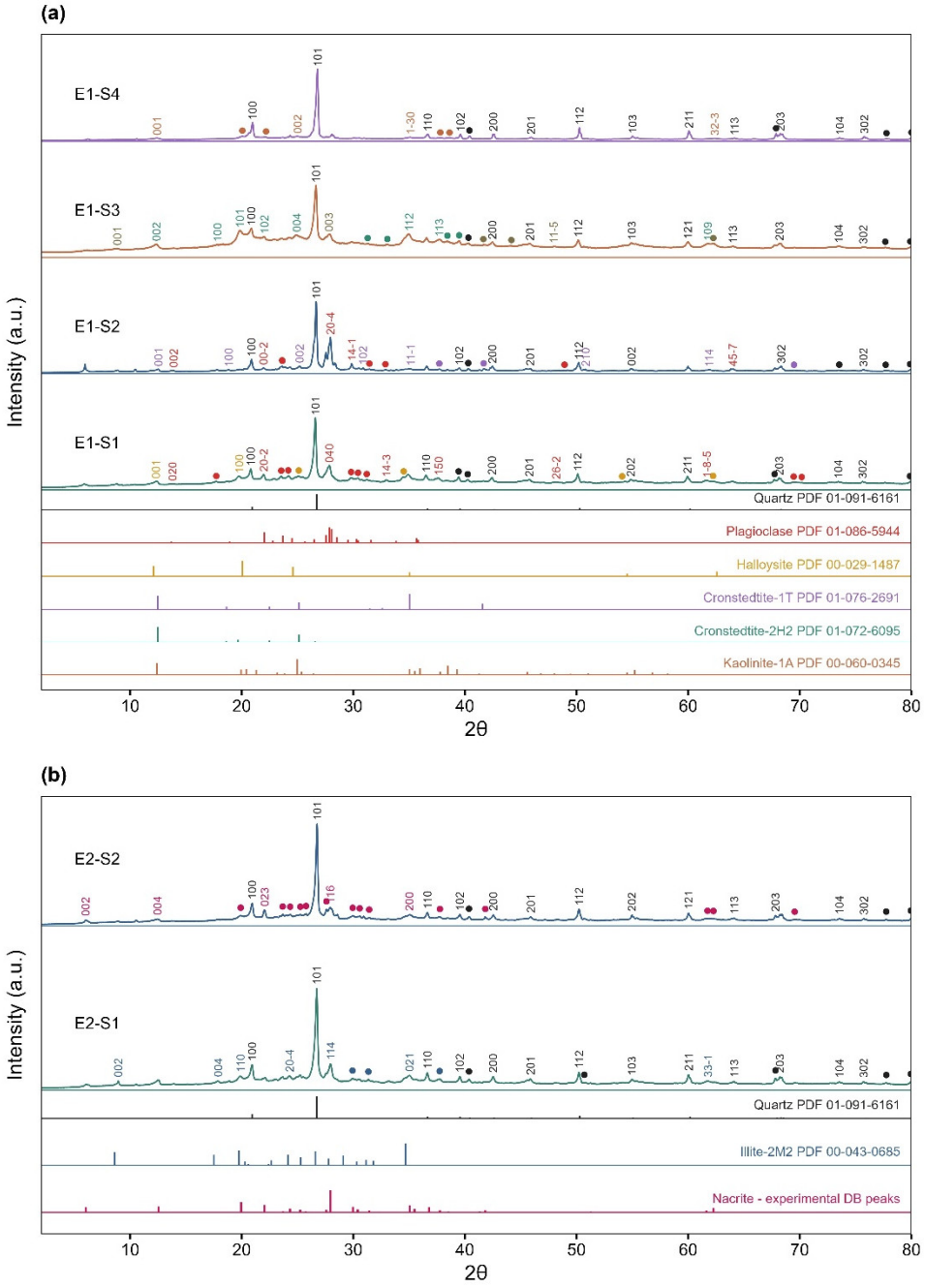


Figure A1. X-ray diffraction patterns of additional sediment samples collected during: (**a**) E1 and (**b**) E2.

References

1. Sonke, J.E.; Angot, H.; Zhang, Y.; Poulain, A.; Björn, E.; Schartup, A. Global Change Effects on Biogeochemical Mercury Cycling. *Ambio* **2023**, *52*, 853–876. https://doi.org/10.1007/s13280-023-01855-y.
2. Aldous, A.R.; Tear, T.; Fernandez, L.E. The Global Challenge of Reducing Mercury Contamination from Artisanal and Small-Scale Gold Mining (ASGM): Evaluating Solutions Using Generic Theories of Change. *Ecotoxicology* **2024**, *33*, 506–517. https://doi.org/10.1007/s10646-024-02741-3.
3. Charkiewicz, A.E.; Omeljaniuk, W.J.; Garley, M.; Nikliński, J. Mercury Exposure and Health Effects: What Do We Really Know? *Int. J. Mol. Sci.* **2025**, *26*, 1–26. https://doi.org/10.3390/ijms26052326.
4. Secretariat of the Minamata Convention on Mercury. *Minamata Convention on Mercury*; Secretariat of the Minamata Convention on Mercury: Geneva, Switzerland, 2024; pp. 582–616.

5. Martoredjo, I.; Calvão Santos, L.B.; Vilhena, J.C.E.; Rodrigues, A.B.L.; de Almeida, A.; Sousa Passos, C.J.; Florentino, A.C. Trends in Mercury Contamination Distribution among Human and Animal Populations in the Amazon Region. *Toxics* **2024**, *12*, 204. https://doi.org/10.3390/toxics12030204.
6. de Castro Paiva, T.; Dary, E.P.; Pestana, I.A.; Amadio, S.A.; Malm, O.; Kasper, D. Flood-Pulse and Trophic Position Modulate Mercury Concentrations in Fishes from an Amazon Floodplain Lake. *Environ. Res.* **2022**, *215*, 114307. https://doi.org/10.1016/j.envres.2022.114307.
7. Domingues, V.S.; Colmenero, C.; Vinograd, M.; Oliveira-da-Costa, M.; Balbueno, R. Mercury Dynamics and Bioaccumulation Risk Assessment in Three Gold Mining-Impacted Amazon River Basins. *Toxics* **2024**, *12*, 1–20. https://doi.org/10.3390/toxics12080599.
8. de Souza, J.P.R.; Garnier, J.; Quintarelli, J.M.; de Sousa Tonhá, M.; Roig, H.L.; Seyler, P.; de Souza, J.R. Adapted Sequential Extraction Protocol to Study Mercury Speciation in Gold Mining Tailings: Implications for Environmental Contamination in the Amazon. *Toxics* **2024**, *12*, 326. https://doi.org/10.3390/toxics12050326.
9. Ignatavičius, G.; Unsal, M.H.; Busher, P.E.; Wołkowicz, S.; Satkūnas, J.; Šulijienė, G.; Valskys, V. Geochemistry of Mercury in Soils and Water Sediments. *AIMS Environ. Sci.* **2022**, *9*, 277–297. https://doi.org/10.3934/ENVIRONSCI.2022019.
10. Nyholt, K.; Jardine, T.D.; Villamarín, F.; Jacobi, C.M.; Hawes, J.E.; Campos-Silva, J.V.; Srayko, S.; Magnusson, W.E. High Rates of Mercury Biomagnification in Fish from Amazonian Floodplain-Lake Food Webs. *Sci. Total Environ.* **2022**, *833*, 155161. https://doi.org/10.1016/j.scitotenv.2022.155161.
11. Escobar-Camacho, D.; Rosero-López, D.; Ruiz-Urigüen, M.; Barragán, K.S.; Carpintero-Salvador, N.; Daza, J.R.; Aldous, A.; Benítez, S.; Tear, T.; Encalada, A.C. Mercury in Aquatic Ecosystems of Two Indigenous Communities in the Piedmont Ecuadorian Amazon: Evidence from Fish, Water, and Sediments. *Ecotoxicology* **2024**, *33*, 440–456. https://doi.org/10.1007/s10646-024-02764-w.
12. de Paula Gutiérrez, B.F.; Agudelo, C.A.R. Fish as Bioindicators: Coal and Mercury Pollution in Colombia's Ecosystems. *Environ. Sci. Pollut. Res.* **2020**, *27*, 27541–27562.
13. United Nations Office on Drugs and Crime (UNODC). *Colombia Explotación de Oro de Aluvión*; UNODC: Bogotá, Colombia, 2022.
14. Gutiérrez-Mosquera, H.; Marrugo-Negrete, J.; Díez, S.; Morales-Mira, G.; Montoya-Jaramillo, L.J.; Jonathan, M.P. Mercury Distribution in Different Environmental Matrices in Aquatic Systems of Abandoned Gold Mines, Western Colombia: Focus on Human Health. *J. Hazard. Mater.* **2021**, *404*, 124080. https://doi.org/10.1016/j.jhazmat.2020.124080.
15. Instituto de Hidrología, Meteorología y Estudios Ambientales (IDEAM). *Instructivo de Toma y Preservación de Muestras de Sedimentos y Agua Superficial Para La Red de Referencia Nacional de Calidad de Agua Del IDEAM*; IDEAM: Bogotá, Colombia, 2026.
16. ICONTEC. *Guía Técnica Colombiana GTC25: Water Quality. Sampling of Aquatic Communities*, 2nd ed.; ICONTEC: Bogotá, Colombia, 2023.
17. Lipps, W.C.; Braun-Howland, E.B.; Baxter, T.E. *Standard Methods for the Examination of Water and Wastewater*; American Public Health Association: Washington, DC, USA, 2023. ISBN 9780875532998.
18. Canadian Council of Ministers of the Environment (CCME). *Canadian Sediment Quality Guidelines for the Protection of Aquatic Life: Chromium*; CCME: Winnipeg, MB, Canada, 1999.
19. Gomes, P.R.; Pestana, I.A.; de Almeida, M.G.; de Oliveira, B.C.V.; de Rezende, C.E. Effects of Illegal Gold Mining on Hg Concentrations in Water, Pistia Stratiotes, Suspended Particulate Matter, and Bottom Sediments of Two Impacted Rivers (Paraíba Do Sul River and Muriaé River), Southeastern, Brazil. *Environ. Monit. Assess.* **2022**, *194*, 1–16. https://doi.org/10.1007/s10661-022-10477-y.
20. Rico-Sánchez, A.E.; Rodríguez-Romero, A.J.; Sedeño-Díaz, J.E.; López-López, E.; Sundermann, A. Aquatic Macroinvertebrate Assemblages in Rivers Influenced by Mining Activities. *Sci. Rep.* **2022**, *12*, 1–14. https://doi.org/10.1038/s41598-022-06869-2.
21. Ministerio de Ambiente, Vivienda y Desarrollo Territorial. *Decree 3930 DE 2010*; Ministerio de Ambiente, Vivienda y Desarrollo Territorial: Bogotá, Colombia, 2010; p. 19.
22. Ministerio de Ambiente, Vivienda y Desarrollo Territorial. *Resolución 2115 de 22 de Junio de 2007*; Ministerio de Ambiente, Vivienda y Desarrollo Territorial: Bogotá, Colombia, 2007; p. 37.
23. World Health Organization (WHO). *Guidelines for Drinking-Water Quality*; WHO: Geneva, Switzerland, 2022; Volume 4. ISBN 1111111111.
24. Escobar, M.C.; Niño-Garcia, J.P.; Acosta, A.; Núñez-Avellaneda, M.; Agudelo Córdoba, E.; Caicedo, J.; Acosta-Gonzalez, A.; Vasquez, Y.; Marrugo-Negrete, J.L.; Marqués, S.; et al. Mercury Biomagnification and Microbial Adaptation in a Mining-Impacted Amazonian River. *J. Hazard. Mater.* **2025**, *495*, 138989. https://doi.org/10.1016/j.jhazmat.2025.138989.

25. U.S. Environmental Protection Agency (EPA) National Recommended Water Quality Criteria - Aquatic Life Criteria Table. [[Online] Available In: <U.S. EPA Aquatic Life Criteria Table>. **2026**..
26. Seelen, E.; Liem-Nguyen, V.; Wünsch, U.; Baumann, Z.; Mason, R.; Skyllberg, U.; Björn, E. Dissolved Organic Matter Thiol Concentrations Determine Methylmercury Bioavailability across the Terrestrial-Marine Aquatic Continuum. *Nat. Commun.* **2023**, *14*, 1–13. https://doi.org/10.1038/s41467-023-42463-4.
27. Wang, Y.; Liu, J.; Liem-Nguyen, V.; Tian, S.; Zhang, S.; Wang, D.; Jiang, T. Binding Strength of Mercury (II) to Different Dissolved Organic Matter: The Roles of DOM Properties and Sources. *Sci. Total Environ.* **2022**, *807*, 150979. https://doi.org/10.1016/j.scitotenv.2021.150979.
28. Chen, C.; Ting, Y.; Ch'ng, B.L.; Hsi, H.C. Influence of Sulfide, Chloride and Dissolved Organic Matter on Mercury Adsorption by Activated Carbon in Aqueous System. *Sustain. Environ. Res.* **2020**, *30*, 1–15. https://doi.org/10.1186/s42834-020-00065-5.
29. Poulin, B.A.; Tate, M.T.; Janssen, S.E.; Aiken, G.R.; Krabbenhoft, D.P. A Comprehensive Sulfate and DOM Framework to Assess Methylmercury Formation and Risk in Subtropical Wetlands. *Nat. Commun.* **2025**, *16*, 1–13. https://doi.org/10.1038/s41467-025-59581-w.
30. Becerra-Lira, E.; Rodriguez-Achata, L.; Muñoz Ushñahua, A.; Corvera Gomringer, R.; Thomas, E.; Garate-Quispe, J.; Hilares Vargas, L.; Nascimento Herbay, P.R.; Gamarra Miranda, L.A.; Umpiérrez, E.; et al. Spatio-Temporal Trends of Mercury Levels in Alluvial Gold Mining Spoils Areas Monitored between Rainy and Dry Seasons in the Peruvian Amazon. *Environ. Res.* **2024**, *245*, 118073. https://doi.org/10.1016/j.envres.2023.118073.
31. Dabré, D.; Guédron, S.; Maïga, Y.; Jelavic, S.; Campillo, S.; Fin, J.; Sentenac, S.; Bruneel, O.; Ouédraogo, O.; Mason, R. Mercury Transfer and Transformation from Mine Soil to River Sediments: The Potential Role of Amorphous Iron Oxides in Methylation Processes in Southern Burkina Faso. *Environ. Sci. Process. Impacts* **2025**, *27*, 3246–3260. https://doi.org/10.1039/d5em00426h.
32. Ministerio de Salud y Protección Social. *Resolution 122 of 2012: Partial Amendment of Resolution 776 of 2008 Regarding Fishery Products in Colombia.*; Minsalud.gov.co: Bogotá, Colombia, 2012; p. 10.
33. de Oliveira, C.A.C.R.; Morais, K.S.; de Oliveira, J.P.S.; de Oliveira Marques, A.; da Silva, A.B.F.; da Conceição Palheta, D.; Bentes, B. The Use of Fish Diversity and Abundance as Environmental Indicators in a Mining Region in Brazilian Amazonia. *Sci. Rep.* **2026**, *16*, 1–15. https://doi.org/10.1038/s41598-026-43889-8.
34. Cajado, R.A.; de Oliveira, L.S.; da Silva, F.K.S.; Zacardi, D.M.; Andrade, M.C. Effects of Anomalous Climatic Events on the Structure of Fish Larvae Assemblages in the Eastern Amazon. *Front. Environ. Sci.* **2022**, *10*, 1–15. https://doi.org/10.3389/fenvs.2022.1064170.
35. Liu, J.; Li, Y.; Zhang, A.; Zhong, H.; Jiang, H.; Tsui, M.T.K.; Li, M.; Pan, K. Impact of Geochemistry and Microbes on the Methylmercury Production in Mangrove Sediments. *J. Hazard. Mater.* **2024**, *479*, 135627. https://doi.org/10.1016/j.jhazmat.2024.135627.
36. Azevedo, L.S.; Pestana, I.A.; Almeida, M.G.; Ferreira da Costa Nery, A.; Bastos, W.R.; Magalhães Souza, C.M. Mercury Biomagnification in an Ichthyic Food Chain of an Amazon Floodplain Lake (Puruzinho Lake): Influence of Seasonality and Food Chain Modeling. *Ecotoxicol. Environ. Saf.* **2021**, *207*, 111249. https://doi.org/10.1016/j.ecoenv.2020.111249.
37. Salazar-Camacho, C.; Salas-Moreno, M.; Paternina-Uribe, R.; Marrugo-Negrete, J.; Díez, S. Mercury Species in Fish from a Tropical River Highly Impacted by Gold Mining at the Colombian Pacific Region. *Chemosphere* **2021**, *264*, 128478. https://doi.org/10.1016/j.chemosphere.2020.128478.
38. Malov, V.; Subetto, D.; Strakhovenko, V.; Ovdina, E.; Belkina, N. Distribution of Mercury in the Water-Suspended Matter-Bottom Sediments System of the Lake Onego Water Area. *Minerals* **2022**, *12*, 1410. https://doi.org/10.3390/min12111410.
39. Wang, P.; Shen, X.; Qiu, S.; Zhang, L.; Ma, Y.; Liang, J. Clay-Based Materials for Heavy Metals Adsorption: Mechanisms, Advancements, and Future Prospects in Environmental Remediation. *Crystals* **2024**, *14*, 1046. https://doi.org/10.3390/cryst14121046.
40. Gerson, J.R.; Szponar, N.; Zambrano, A.A.; Bergquist, B.; Broadbent, E.; Driscoll, C.T.; Erkenswick, G.; Evers, D.C.; Fernandez, L.E.; Hsu-Kim, H.; et al. Amazon Forests Capture High Levels of Atmospheric Mercury Pollution from Artisanal Gold Mining. *Nat. Commun.* **2022**, *13*, 1–10. https://doi.org/10.1038/s41467-022-27997-3.
41. Olivero-Verbel, J.; Carranza-Lopez, L.; Caballero-Gallardo, K.; Ripoll-Arboleda, A.; Muñoz-Sosa, D. Human Exposure and Risk Assessment Associated with Mercury Pollution in the Caqueta River, Colombian Amazon. *Environ. Sci. Pollut. Res.* **2016**, *23*, 20761–20771. https://doi.org/10.1007/s11356-016-7255-3.
42. Vargas Licona, S.P.; Marrugo Negrete, J.L. Mercurio, Metilmercurio y Otros Metales Pesados En Peces de Colombia: Riesgo Por Ingesta. *Acta Biolo. Colomb.* **2019**, *24*, 232–242. https://doi.org/10.15446/abc.v24n2.74128.

43. Paiva, T.d.C.; Pestana, I.A.; Miranda, L.N.L.; de Carvalho, G.O.; Bastos, W.R.; Kasper, D. Mercury Scenario in Fish from the Amazon Basin: Exploring the Interplay of Social Groups and Environmental Diversity. *Toxics* **2025**, *13*, 1–19. https://doi.org/10.3390/toxics13070580.
44. Salomão, G.N.; Dall'Agnol, R.; Sahoo, P.K.; de Almeida, G.S.; Amarante, R.T.; Zeferino, L.B.; Lopes, J.P.N.; Souza Filho, P.W.M.e.; da Costa, N.Y.M.; Guimarães, J.T.F.; et al. Changes in the Surface Water Quality of a Tropical Watershed in the Southeastern Amazon Due to the Environmental Impacts of Artisanal Mining. *Environ. Pollut.* **2023**, *329*, 121595. https://doi.org/10.1016/j.envpol.2023.121595.

Disclaimer/Publisher's Note: The statements, opinions and data contained in all publications are solely those of the individual author(s) and contributor(s) and not of MDPI and/or the editor(s). MDPI and/or the editor(s) disclaim responsibility for any injury to people or property resulting from any ideas, methods, instructions or products referred to in the content.